Turkish Journal of Earth Sciences (Turkish J. Earth Sci.), **Vol. 15**, 2006, pp. 47-73. *Copyright ©TÜBİTAK*

Mineral-Chemical Constraints on the Miocene Calc-alkaline and Shoshonitic Volcanic Rocks of Western Turkey: Disequilibrium Phenocryst Assemblages as Indicators of Magma Storage and Mixing Conditions

ERCAN ALDANMAZ

Department of Geological Engineering, Kocaeli University, TR-41040 İzmit, Turkey
(E-mail: ercan.aldanmaz@dunelm.org.uk)

Abstract: Early to Middle Miocene (22 to 15 Ma) volcanic activity across western Turkey produced a series of lavas and pyroclastic deposits with calc-alkaline and shoshonitic affinities. The erupted magmas show a broad range of compositions from basaltic to rhyolitic (48–75 SiO_2 wt%) and are composed of variable phenocryst assemblages. Petrographic and mineral-chemical characteristics suggest that the magmas underwent hydrous crystallization in deep crustal magma chambers that was dominated by plagioclase + pyroxene + pargasitic amphibole fractionation. Subsequent crystallization in shallower magma chambers followed two different trends: (1) anhydrous (pyroxene + plagioclase-dominated); and (2) hydrous (plagioclase + edenitic amphibole + pyroxene-dominated). Application of magnetite-ilmenite, hornblende-plagioclase and two-pyroxene geothermometry to the western Anatolian volcanic rocks has yielded temperature estimates in the range of 585–1086 ºC for the Early Miocene and 768–1095 ºC for the Middle Miocene rocks. Pressure estimates from pyroxene and Al-in-hornblende geobarometers are in the range of 2.1–8.6 kbar for the Early Miocene and 6.5–9.1 kbar for the Middle Miocene rocks. The presence of amphibole with clear signs of disequilibrium, and plagioclase as inclusions in pyroxenes and other phenocryst cores, suggest that magma mixing was operational during the formation of the volcanic suites. Strong compositional variations and reverse zoning patterns in single phenocrysts, as well as considerably variable pressures of crystallization, further indicate that the magmas forming the volcanic suite had a polybaric origin and are the composite products of more than one petrogenetic stage. The observed range of phenocryst assemblages and different compositional trends are likely to have originated from fractionation of magmas with different initial water contents, under variable pressures of crystallization. The repeated occurrence of magmas from different suites during a single period of activity suggests that the magmatic system comprised several conduit systems and magma reservoirs dispersed at different levels of crustal magma chambers. The results suggest that the episodic intrusion of mafic magmas provided the necessary heat and perhaps contributed to the ascent of the magma to shallow crustal depths where it reequilibrated before the onset of eruption.

Key Words: western Anatolia, magma evolution, magma mixing, compositional zoning, disequilibrium parameters, crustal magma chambers

Batı Türkiye Miyosen Kalk-alkalin ve Şoşonitik Volkanik Kayalarının Mineral Kimyasal Özellikleri: Magma Oluşumu ve Karışımı Koşullarının Dengesiz Fenokristal Topluluklarıyla Belirlenmesi

Özet: Batı Türkiye Erken ve Orta Miyosen dönemi (22–15 My) volkanik aktivitesi kalk-alkalin ve şoşonitik özelliklere sahip lav ve piroklastik ürünler oluşturmuştur. Oluşan magmalar bazalttan riyolite kadar değişen (48–75 SiO_2 wt%) geniş bir bileşim aralığı sunar ve değişken fenokristal topluluklarından meydana gelir. Petrografik ve mineral kimyasal özellikleri, magmaların derin magma odası koşullarında plajioklas + piroksen + pargasitik amfibol ayrımlaşma baskın olduğu sulu fazlı bir kristalleşme geçirmiş olduklarına işaret etmektedir. Bunu izleyen ve daha sığ magma odalarında gerçekleşen kristalleşme iki farklı yönelim sunar: (1) susuz (piroksen + plajioklasın baskın olduğu); ve (2) sulu (plajioklas + edenitik amfibol + piroksenin baskın olduğu) ayrımlaşma. Batı Türkiye volkanik kayalarına uygulanan magnetit-ilmenit, hornblend-plajioklas ve çift piroksen jeotermometreleri Erken Miyosen kayaları için tahmini 585–1086 ºC ve Orta Miyosen kayaları için 768–1095 ºC arasında değişen kristalleşme sıcaklığı ortaya koymaktadır. Piroksen ve hornblend-Al jeobarometreleri ise Erken Miyosen kayaları için 2.1–8.6 kbar ve Orta Miyosen kayaları için 6.5–9.1 kbar arasında değişen basınç değerlerine işaret etmektedir. Dengesiz kristalleşme özelliklerine sahip amfibol kristallerinin varlığı ve plajioklas minerallerinin piroksenler ve diğer fenokristallerin içinde bulunuşu, volkanik serilerin oluşumunda magma karışımının etkin olduğunu göstermektedir. Minerallerde gözlenen belirgin tane içi bileşim değişimleri, ters zonlanmalar ve oldukça değişken kristalleşme basınçları, volkanik kayaları oluşturan magmaların polibarik bir kökene sahip olduklarına ve birden fazla

petrojenetik safhadan etkilenmiş kompozit ürünler olduklarına işaret etmektedir. Gözlenen fenokristal toplulukları ve bunların bileşim aralıkları, değişken miktarlarda su içeren magmaların yine değişken kristalleşme basınçlarında ayrışmasıyla uyumludur. Aynı magmatik aktivite devri esnasında farklı magma bileşimlerinin tekrarlanan oluşumları magmatik sitemin farklı kabuk derinliklerinde yeralan magma haznesinden oluştuklarını göstermektedir. Sonuçlar, mafik magmaların magma odalarına tekrarlanan sokulumlarının gerekli ısının oluşumunu sağladığını ve olasılıkla magmaların püskürme öncesi denge haline geçtikleri daha sığ magma odalarına yükselimine katkıda bulunduklarını göstermektedir.

Anahtar Sözcükler: Batı Anadolu, magma evrimi, magma karışımı, bileşim zonlanması, dengesizlik parametereleri, kabuksal magma odaları

Introduction

Extensive volcanic activity has characterized western Turkey and the Aegean Sea region since the Late Eocene. Voluminous volcanic products cover large areas from the Aegean subduction zone through western Anatolia and the Aegean islands into Thrace (Figure 1). Volcanism in the area may be divided into two groups according to the relationship between magma generation and regional tectonic activity: (1) Late Eocene to Recent volcanism related to collision between the Anatolide-Tauride platform and Pontides, and to subsequent orogenic collapse and lithospheric extension; and (2) Late Miocene to Recent volcanism related to northward-dipping subduction of the African plate beneath the Eurasian plate along the Aegean trench. Products of subduction-related volcanism are distributed along the south Aegean arc, from the Cyclades through the Dodecanese provinces to southwestern Anatolia, and have been dated as ~12 Ma to Recent (~3 Ka) (Keller 1983; Wyers & Barton 1987; Robert *et al.* 1992; Allen & Cas 1998). The products of the collision-related (or post-collision) volcanism, however, occupy large areas in the northern part of the Aegean Sea and western Anatolia (e.g., Aldanmaz *et al.* 2000; Yılmaz *et al.* 2001). The post-collision volcanism of western Anatolia is the subject of this study and is here termed "the Late Cenozoic volcanic province of western Anatolia".

The Late Cenozoic volcanic province of western Anatolia comprises a series of calc-alkaline and shoshonitic volcanic products originated from a number of eruptive episodes. In the area the early stage of this activity lasted from the Early Miocene to the Middle Miocene, and was marked by shoshonitic and high-K, calc-alkaline eruptive products that range in composition from basaltic andesite to rhyolite. This episode was associated with uplift and thickened lithosphere, and may have been caused by subsequent orogenic collapse. The later stage, during the Middle Miocene, was marked by less silicic and relatively less potassic (and less phyric) eruptive products which are considered to have originated by melting along localized extensional zones. Published geochemical data indicate that the melt products of both stages originated from subduction-enriched mantle lithospheric sources and were subsequently modified by extensive magma-crust interaction (e.g., Aldanmaz *et al.* 2000).

In this contribution, an attempt has been made to document the pre-eruption evolution of magmas in an effort to constrain the intensive parameters of the ascending magmas, such as pressure and temperature, and plumbing conditions. A comprehensive petrologic and mineral-chemical investigation has been made to infer the magma-chamber conditions in the mixed magmas. I particularly use the evidence for multiple styles of mixing, the compositions of coexisting phenocryst phases, and the compositional zoning in the eruptive products of western Anatolia to provide insights into the nature of magmatic processes, with a special effort to evaluate the role of magma mixing in the petrogenesis of the calc-alkaline and shoshonitic magmatic series.

Geological Background

The western Anatolia region is an active continental extensional zone that is characterized by relatively high surface heat flow and thermal uplift. Regional tectonic and magmatic activity during much of the Miocene period is considered to have been largely influenced by lithospheric spreading and thinning subsequent to earlier plate collision and stacking (e.g., Dewey *et al.* 1986; Aldanmaz *et al.* 2000 and references therein). In this region, the products of extensive volcanic activity cover large areas to the north of the Menderes Massif. The geological characteristics and tectono-magmatic evolution of the region have been described in detail in a number of previous studies (e.g., Güleç 1991; Seyitoğlu *et al.* 1997; Aldanmaz *et al.* 2000, 2005, 2006; Aldanmaz 2002;

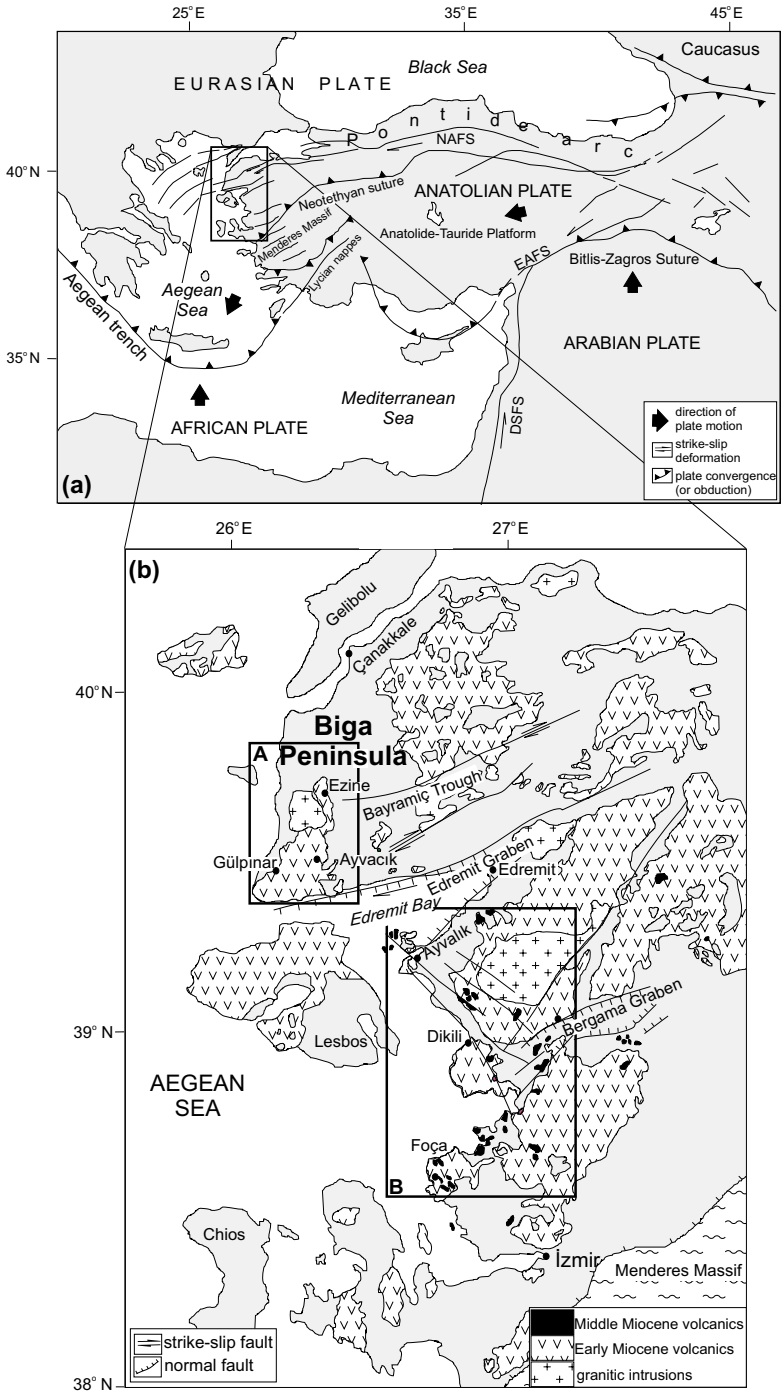

Figure 1. (a) Map showing tectonic boundaries and plates motion in eastern Mediterranean (based on data from Dewey *et al.* 1986; Şengör & Yılmaz 1981; Bozkurt 2001). (b) Simplified map of western Anatolia showing the distribution of the Early to Middle Miocene magmatic products (from Aldanmaz *et al.* 2000). The northern (A) and southern (B) areas are indicated in the map. (NAFS – North Anatolian Fault System; EAFS – East Anatolian Fault System; DSFS – Dead Sea Fault System).

Yılmaz *et al.* 2001; Bozkurt 2001; Köprübaşı & Aldanmaz 2004; Bozkurt & Mittwede 2005; Erkül *et al.* 2005; Tokçaer *et al.* 2005; Yücel-Öztürk *et al.* 2005), and only a brief description will be given here. Aldanmaz *et al.* (2000) have investigated the calc-alkaline and shoshonitic volcanic products in two different localities: (1) the Ezine-Gülpınar-Ayvacık area, which is located on the Biga Peninsula (referred to here as the northern area); and (2) the Dikili-Ayvalık-Bergama area, which is located farther south (referred to here as the southern area; Figure 1b).

Field observations, volcanological characteristics and published radiometric data show that major volcanic activity took place both in the northern and southern areas during the Early Miocene, and produced a considerable volume of pyroclastic deposits and lavas of intermediate to acidic composition (Aldanmaz *et al.* 2000). The early stage of activity began with lava flows and continued with lava and pyroclastic successions, most of which originated from fissure eruptions. The large volumes of these lavas are andesitic to rhyolitic in composition and are characterized by their high phenocryst contents. The pyroclastic deposits are generally large ignimbrite sheets accompanied by minor debris and ash-flow deposits.

Early Miocene is the oldest known age for volcanic rocks of the study area (21 Ma; Aldanmaz *et al.* 2000), but pre-Miocene volcanic rocks have been reported from some other parts of the Biga Peninsula (Ercan *et al.* 1984, 1995). In the northern area, the early stage of volcanic activity was followed by abundant dyke injections, mainly microporphyritic andesites and basaltic andesites in composition. Aldanmaz *et al.* (2000) have reported a K-Ar age of 19 Ma for the dyke injections.

In the southern area, the volcanic activity continued into the Middle Miocene, with a gradual change in the eruptive style and rock compositions. The Middle Miocene activity is marked by aphyric or weakly porphyritic lava flows, domes and dykes of mafic to intermediate composition; these are volumetrically less abundant than the earlier lavas. Pyroclastic eruptive products are absent in this period. The lavas mostly lie in the small localized extensional zones bounded by E–W- or NE–SW-oriented fault systems, indicating a relationship between volcanism and the local extensional tectonic regime in the area during this period. The published K-Ar data show that the Middle Miocene volcanic activity in the southern area lasted until 15 Ma (Borsi *et al.* 1972; Aldanmaz *et al.* 2000).

Rock Description

The products of the Early to Middle Miocene volcanic activity in western Anatolia are dominated by calc-alkaline and shoshonitic rock varieties. The erupted magmas show a wide range of compositions, from basaltic to rhyolitic, with SiO_2 contents ranging between 48 and 78 wt% (Figure 2). A time-integrated change in rock chemistry, however, is obvious as the volcanic activity began with acidic-intermediate compositions during the Early Miocene and shifted toward less silicic compositions during the Middle Miocene (Figure 2; Aldanmaz *et al.* 2000).

The andesitic and dacitic lavas of the calc-alkaline and shoshonitic suites contain about 35 to 50 vol% phenocrysts. Typical phenocrysts are plagioclase, clinopyroxene, orthopyroxene, amphibole, K-feldspar, biotite and Fe-Ti oxides (magnetite-ilmenite). Plagioclase is the most abundant phenocryst phase, accounting for ~65–70 vol% of the phenocryst assemblage in most of the rocks. In most of the Early Miocene calc-alkaline and shoshonitic lavas from the southern area, clinopyroxene is abundant and amphibole and biotite represent hydrous assemblages, while orthopyroxene is a scarce phenocryst phase. However, amphibole is extremely scarce in rocks of the same age from the northern area, and is observed only in a few lavas as disrupted xenocrysts, with clear signs of disequilibrium (e.g., reaction rims). The typical assemblage from the northern area is plagioclase with orthopyroxene, clinopyroxene, K-feldspar, oxides and biotite.

Olivine and quartz are scarce and present only in a few lavas of the mafic and felsic end-member products of the Early Miocene rocks, respectively. Some rocks also contain apatite and zircon. The more acidic dacitic and rhyolitic lavas contain titanite in addition to the other mineral phases. Porphyritic textures predominate in the most silicic andesites and dacites. Textural relations, such as resorption along grain boundaries, oscillatory zoning in plagioclase and clinopyroxene, and existence of hornblende xenocrysts with clinopyroxene reaction rims, suggest that the major population of the phenocrysts are in disequilibrium with their host liquid.

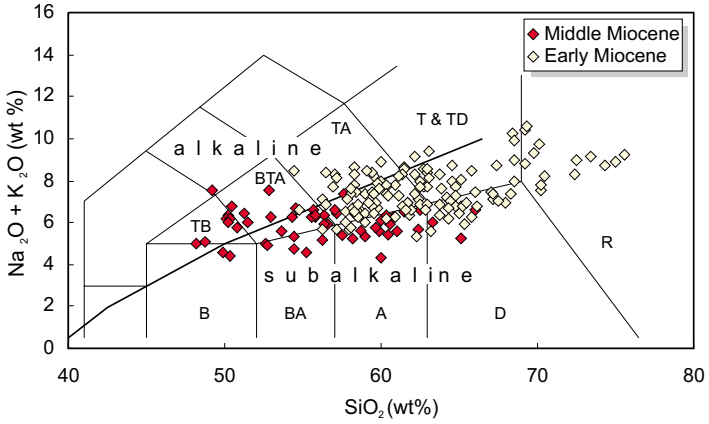

Figure 2. Classification of the Early to Middle Miocene volcanic rocks from western Anatolia (based on the whole-rock geochemical data of Aldanmaz *et al.* 2000) on a total alkali versus silica (TAS) diagram of LeBas *et al.* (1986). Dashed line is boundary between alkaline and subalkaline rocks of Irvine & Baragar (1971). (B– basalt; BA– basaltic andesite; A– andesite; D– dacite; R– rhyolite; TB– trachybasalt; BTA– basaltic trachyandesite; TA– trachyandesite; T– trachyte; TD– trachydacite).

The small volume basaltic andesite and andesitic lavas of the later-stage (Middle Miocene) calc-alkaline series display typical quench textures, with abundant phenocrysts embedded in a fine-grained groundmass. Glass is preserved in very few cases and groundmass consists mainly of microcrystalline plagioclase, clinopyroxene, Fe-Ti oxides and, in places, K-feldspar. Plagioclase, zoned clinopyroxene, olivine and subordinate orthopyroxene are the ubiquitous phenocryst phases, and occur with minor phlogopite, Fe-Ti oxides (magnetite and ilmenite) and scarce Ti-rich biotite. Some samples also include a considerable amount of sanidine in the groundmass. The rocks can be distinguished from the earlier lavas by their more mafic mineral contents.

Mineral Chemistry

Mineral-chemical analyses were made on 26 polished thin sections. Thin sections were prepared at the University of Durham, and carbon coated at the University of Edinburgh. Analyses were performed in Edinburgh on a CAMECA CAMEBAX electron microprobe using natural minerals as standards. Operating conditions were ~20 kV acceleration voltage, ~2/nA beam current, 30s pk count, 15 s b/g count, 1 mm^2 spot size and a 25 mm^2 retard beam size. The representative mineral-chemical data for the whole suite is given in Tables 1–7 with rock types and sample localities given in Table 8, and mineral phases are chemically described below.

Plagioclase

Plagioclase phenocrysts show variable types of compositional zoning – normal, reverse, and oscillatory, or a complex combination of these three types. Thus, at least two points of a single plagioclase crystal (one near the rim and one in the core) were analyzed. The compositional range of plagioclases representing the studied rock suites is given in Table 1. The majority of plagioclase crystals are andesine, labradorite and bytownite in composition.

The compositions of plagioclase generally correlate negatively with the silica contents of the host rocks (Figure 3a). The most An-rich plagioclase phenocrysts occur in the Middle Miocene basaltic lavas and dykes of the southern area, while the most An-poor crystals are from the Early Miocene acidic, porphyritic lavas. The phenocrysts are mostly within a range of 5–25 mole %An unit, although extreme core-to-rim zoning (up to 45 mole % An unit) is observed in some of the phenocrysts.

Table 1. Representative microprobe analyses of plagioclase phenocrysts and microphenocrysts in volcanic rocks of western Anatolia.

Plagioclase																				
Sample no. (c)ore/(r)im	EA409		EA348		EA109		EA143		EA101		EA313		EA112		EA316		EA99		EA147	
	c	r	c	r	c	r	c	r	c	r	c	r	c	r	c	r	c	r	c	r
SiO_2	45.67	46.83	48.56	52.83	52.39	52.91	50.17	51.15	48.63	50.10	50.85	48.66	48.22	55.89	59.03	58.42	57.33	59.23	55.91	57.25
Al_2O_3	33.58	32.80	30.96	27.97	29.01	28.35	29.90	29.40	31.02	30.02	30.08	31.90	31.29	26.48	25.23	25.58	25.84	24.80	26.63	26.09
FeO	0.61	0.58	0.84	1.07	0.42	0.61	0.51	0.52	0.51	0.51	0.67	0.49	0.45	0.45	0.23	0.30	0.24	0.28	0.26	0.32
CaO	17.57	16.71	15.11	11.71	12.05	11.80	13.74	13.01	14.88	13.66	13.57	15.31	15.26	9.22	7.45	7.80	8.21	6.99	9.14	8.57
Na_2O	1.50	1.99	2.85	4.66	4.34	4.18	3.45	3.75	2.83	3.38	3.63	2.66	2.72	5.49	6.85	6.39	6.57	7.14	5.94	6.31
K_2O	0.06	0.10	0.22	0.31	0.31	0.59	0.45	0.52	0.31	0.40	0.29	0.16	0.22	0.85	0.76	0.69	0.51	0.68	0.48	0.57
Total	98.97	99.02	98.54	98.55	98.52	98.46	98.21	98.35	98.16	98.06	99.08	99.19	98.16	98.37	99.54	99.19	98.70	99.12	98.36	99.11
Si	2.116	2.164	2.256	2.431	2.408	2.434	2.330	2.366	2.267	2.328	2.323	2.235	2.250	2.557	2.647	2.626	2.602	2.668	2.555	2.592
Al	1.834	1.786	1.695	1.517	1.571	1.537	1.636	1.603	1.704	1.644	1.620	1.726	1.721	1.427	1.333	1.356	1.383	1.317	1.434	1.393
Fe	0.047	0.045	0.029	0.037	0.015	0.024	0.020	0.020	0.020	0.020	0.051	0.038	0.018	0.017	0.017	0.023	0.008	0.010	0.010	0.011
Ca	0.872	0.827	0.752	0.577	0.593	0.582	0.683	0.644	0.743	0.680	0.664	0.753	0.763	0.452	0.358	0.376	0.400	0.337	0.447	0.416
Na	0.134	0.179	0.257	0.416	0.387	0.373	0.310	0.336	0.255	0.304	0.322	0.237	0.246	0.487	0.595	0.557	0.579	0.624	0.526	0.554
K	0.003	0.006	0.013	0.018	0.018	0.035	0.026	0.031	0.018	0.024	0.017	0.010	0.013	0.050	0.043	0.040	0.030	0.039	0.028	0.033
Total	5.01	5.01	5.00	5.00	4.99	4.99	5.01	5.00	5.01	5.00	5.00	5.00	5.01	4.99	4.99	4.98	5.00	5.00	5.00	5.00
An	86.4	81.8	73.6	57.1	59.4	58.8	67.0	63.7	73.1	67.5	66.3	75.4	74.7	45.7	35.9	38.6	39.6	33.7	44.7	41.5
Ab	13.3	17.7	25.1	41.1	38.8	37.7	30.4	33.2	25.1	30.2	32.1	23.7	24.1	49.2	59.7	57.3	57.4	62.4	52.5	55.2
Or	0.3	0.6	1.3	1.8	1.8	3.5	2.6	3.1	1.8	2.4	1.7	1.0	1.3	5.1	4.4	4.1	3.0	3.9	2.8	3.3

In Figure 3b, the Ca# [= Ca/(Ca + Na)] of plagioclase phenocrysts are plotted against the Ca# of whole-rock compositions to assess whether the plagioclase phenocrysts are in equilibrium with their host rocks. To apply this, however, only samples that are likely to have been unaffected by phenocryst accumulation were chosen. Application of plagioclase-melt equilibria was therefore restricted to the Middle Miocene basic and intermediate samples as well as some phenocryst-poor Early Miocene rocks. Theoretical curves highlight approximate equilibrium partitioning of Ca and Na between plagioclase and liquid. For values of equilibrium partitioning, which is given by the equation of $[^{Ca\text{-}Na}KD = (^{plag}X_{Ca} * ^{liq}X_{Na})/(^{plag}X_{Na} * ^{liq}X_{Ca})]$, a range of values from 2 to 5 were plotted following the experimental results of Baker & Eggler (1987), Housh & Luhr (1991), Sisson & Grove (1993) and Panjasawatwong *et al.* (1995). These experimental studies have shown that the equilibrium partitioning (K_D) of Ca and Na between plagioclase and liquid is generally between 2 and 5 for basaltic to dacitic melts crystallized under H_2O-undersaturated to H_2O-saturated conditions (at 2–10 kbar). For H_2O-saturated melts, K_D values increase with increasing melt-H_2O contents, and for H_2O-undersaturated melts K_D values appear to be independent of melt- H_2O content and range mostly between 2 and 4.

The majority of plagioclase phenocrysts from the Early Miocene rocks display clear evidence of disequilibrium as they are too Na-rich to have crystallized from a liquid similar in composition to their host rocks (Figure 3b). Plagioclase phenocrysts from the Middle Miocene lavas, however, are mostly in equilibrium with liquids compositionally similar to their host rocks as the equilibrium partitioning (K_D) of Ca and Na between plagioclase and liquid remains within the range of 2–5 (Figure 3b). Some plagioclase phenocrysts, however, are too Ca-rich to have crystallized from a liquid compositionally similar to their host rock. The experimental studies of Sisson & Grove (1993) and Panjasawatwong *et al.* (1995) demonstrated that the composition of liquidus plagioclase is mainly controlled by the Ca# and H_2O content of the melt from which the plagioclase is crystallized. As discussed by the same authors, the origin of the An-rich phenocrysts must involve crystallization from melts with either extremely high CaO/Na_2O ratio (>8) or high H_2O contents (~6 wt%) or both. Crystallization of highly An-rich plagioclase in

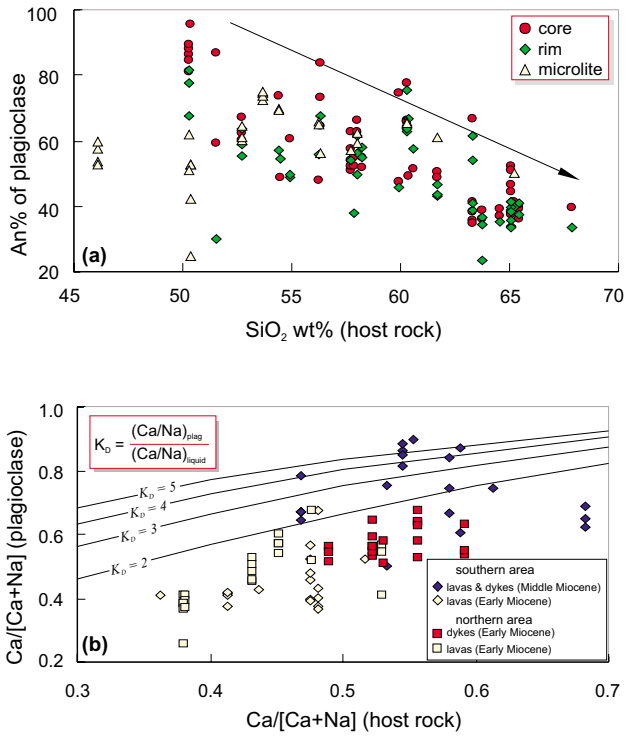

Figure 3. (a) Anorthite contents of core and rim plagioclase and groundmass microlites plotted against silica contents of their host rocks. (b) Ca-numbers (Ca/[Ca+Na]) for plagioclase phenocrysts plotted against Ca-number of host rocks. The curves represent equilibrium values of $^{Ca/Na}KD_{min/liq}$ for hydrous melts based on experimental studies of Baker & Eggler (1987), Housh & Luhr (1991), Sisson & Grove (1993) and Panjasawatwong *et al.* (1995).

most of the mafic-intermediate rocks cannot be explained solely by high CaO/Na_2O ratio of melt because of the apparent negative correlation between the Ca# of plagioclase and host rock (Figure 3b). The high melt H_2O contents might therefore be responsible for the existence of highly An-rich plagioclases in these rocks. Supporting this idea is the presence of hydrous mineral phases (e.g., phlogopite) in some of the Middle Miocene basaltic rocks.

Pyroxenes

Clinopyroxene is one of the most abundant mineral phases in the mafic-intermadiate, calc-alkaline and shoshonitic rocks from both areas. It occurs as large (up to 10 mm) isolated phenocrysts, glomerocrysts, microphenocrysts, and as a groundmass phase. Orthopyroxene is present in most of the calc-alkaline and

shoshonitic rocks of the northern area, while it is a scarce phenocryst phase in rocks of the southern area. The compositions of clinopyroxenes are predominantly diopside, salite, endiopside and augite, whilst orthopyroxenes from the northern area classify mostly as bronzite and hypersthene, according to the I.M.A. classification (Morimoto 1989) (Tables 2 & 3).

Larger clinopyroxene crystals typically show fine oscillatory zoning with broad overall zoning, from Mg-rich cores to more Fe-enriched rims. In some cases, zoning is reverse for both types of pyroxenes, and there is more compositional variation among crystals than within them (Figure 4a, b). Reverse zoning of phenocrysts can be explained by a number of processes including: (1) decompression during magma ascent (Kontak *et al.* 1984); (2) more oxidizing conditions during later stages of crystallization (Luhr & Carmicheal 1980; Grunder & Mahood 1988); or (3) magma mixing (Nixon & Pearce 1987). Sector zoning also occurs in some samples and can be interpreted to have originated from rapid crystal growth (Morrice & Gill 1986).

The Al/Ti ratios in clinopyroxenes from most of the calc-alkaline and shoshonitic rocks increase with decreasing Fs contents from the Early Miocene acidic-intermediate rocks towards the Middle Miocene intermediate-basic rocks (Table 2; Figure 5). This may reflect a greater rate of depletion in Al contained in plagioclase than that of Ti in ilmenite or titanomagnetite in plagioclase-dominated fractionation for the earlier formed rocks due to the lack of ilmenite and titanomagnetite in these rocks. Elevated ratios of Al/Ti in clinopyroxenes of the Middle Miocene rocks coincide with the appearance of ilmenite with extremely low Al/Ti ratios, requiring removal of only a small amount of ilmenite to cause rapid depletion of Ti, and hence increase in Al/Ti ratios even in liquids fractionating plagioclase (Table 2).

Experimental and petrological studies have demonstrated that partitioning of minor elements (e.g., Ti and Al) in pyroxene is strongly growth-rate dependent, although equilibrium partitioning of Ca, Mg and Fe may not be seriously affected by cooling rates (Gamble & Taylor 1980). In particular, high cooling rates favour crystallization of pyroxene with elevated Ti and Al contents (Figure 5a). The existence of Ti- and Al-rich microphenocrysts with high Al/Ti ratios in some of the Middle Miocene basaltic dykes from the southern area therefore probably reflect more elevated cooling rates. This is also consistent with the aphyric or weakly porphyritic nature of these rocks.

Notably, clinopyroxenes of the acidic-intermediate rocks from the southern area are in general enriched in MnO at a given Fs content relative to those of the more mafic Middle Miocene lavas and dykes (Figure 5b). A similar relationship is observed between pyroxenes of the Early Miocene rocks of the northern area, insofar as clinopyroxenes of the highly porphyritic lavas are more enriched in MnO than those of the dyke swarms (Figure 5b). Since Mn^{2+} can substitute for Fe^{2+}, not only in pyroxene, but also in olivine and/or Fe-Ti oxides, the observed linear relationship may be explained by olivine crystallization (with or without Fe-Ti oxides) prior to pyroxene crystallization for the later-formed volcanic rocks of the two areas. This is also supported by the existence of olivine phenocrysts in the dyke swarms of the area.

Amphibole

Amphibole occurs as an abundant mineral phase in most of the Early Miocene acidic-intermediate rocks from the southern area. The main populations of crystals are very large (0.3–1.0 cm), green to brown, and euhedral. Some intermediate rocks of Middle Miocene age of the southern area and Early Miocene age of the northern area also include scarce amphibole xenocrysts with clear signs of disequilibrium (e.g., strong reaction rims and compositional zoning). Reaction rims developed at the expense of large amphibole crystals, where they were in contact with the melt. The origin of these rims can be interpreted as breakdown of amphibole during slow magma ascent from the storage zone at depth (e.g., Rutherford *et al.* 1998). In some cases, amphibole is only represented by occasional remnants in opacite patches, or is altered to masses of small crystals of clinopyroxene + plagioclase + Fe-Ti oxides, probably as a consequence of decompression reactions (e.g., Foden & Green 1992).

The amphibole phenocrysts in the western Anatolian volcanic suites have $(Ca + Na)_{M4} > 1.34$ and $(Na)_{M4} < 0.67$, and thus are calcic amphiboles according to the classification scheme of Leake *et al.* (1997). On the classification diagram of Hawthorne (1981), two compositionally distinct ranges can be identified: (1) edenites and (2) pargasites (Figure 6). Amphibole

Table 2. Representative microprobe analyses of clinopyroxene phenocrysts and microphenocrysts in volcanic rocks of western Anatolia.

Clinopyroxene																				
Sample no. (c)ore/(r)im	EA409		EA350		EA348		EA134		EA109		EA143		EA101		EA313		EA316		EA112	
	c	r	c	r	c	r	c	r	c	r	c	r	c	r	c	r	c	r	c	r
SiO_2	49.33	51.01	52.73	52.32	51.29	51.98	52.29	51.54	46.56	49.01	50.58	50.19	50.56	51.04	52.89	50.99	52.53	48.95	50.56	50.36
TiO_2	1.19	0.60	0.53	0.62	0.42	0.35	0.32	0.42	1.41	1.09	0.85	0.82	0.69	0.42	0.25	0.49	0.15	0.90	0.39	0.44
Al_2O_3	4.81	3.43	1.15	1.18	2.43	2.05	2.18	2.61	6.10	2.89	2.85	3.15	2.00	2.61	1.43	3.58	0.95	5.18	2.21	2.30
FeO	6.76	4.28	4.41	4.34	5.49	5.66	3.28	4.05	8.54	9.04	6.71	6.68	7.63	6.05	5.89	4.92	8.21	7.02	9.39	8.99
MnO	0.14	0.10	0.12	0.13	0.17	0.18	0.11	0.11	0.21	0.24	0.19	0.22	0.26	0.11	0.23	0.15	0.63	0.18	0.51	0.50
MgO	14.02	15.74	17.09	17.34	16.62	17.26	16.62	16.12	12.00	13.14	15.04	15.29	15.60	16.12	17.98	15.88	13.94	14.13	13.52	12.96
CaO	22.60	22.98	22.78	22.23	21.97	21.26	23.13	22.94	21.91	21.70	20.97	21.13	20.44	22.94	19.44	22.13	22.68	21.79	20.88	21.60
Na_2O	0.27	0.27	0.15	0.15	0.22	0.21	0.20	0.20	0.34	0.37	0.32	0.33	0.27	0.20	0.20	0.34	0.33	0.27	0.47	0.49
Total	99.12	98.41	98.96	98.31	98.61	98.95	98.13	97.99	97.07	97.48	97.51	97.81	97.43	99.49	98.30	98.49	99.41	98.41	97.92	97.64
Si	1.849	1.900	1.941	1.937	1.899	1.916	1.942	1.925	1.792	1.878	1.915	1.897	1.923	1.925	1.963	1.900	1.973	1.845	1.933	1.932
Ti	0.034	0.017	0.015	0.017	0.012	0.010	0.009	0.012	0.041	0.031	0.024	0.023	0.020	0.012	0.007	0.014	0.004	0.025	0.011	0.013
Al	0.213	0.151	0.050	0.051	0.106	0.089	0.096	0.115	0.276	0.130	0.127	0.140	0.090	0.115	0.063	0.157	0.042	0.230	0.100	0.104
Fe	0.212	0.133	0.131	0.130	0.161	0.167	0.102	0.127	0.266	0.281	0.212	0.211	0.243	0.198	0.183	0.153	0.258	0.221	0.300	0.288
Mn	0.004	0.003	0.004	0.004	0.005	0.006	0.003	0.004	0.007	0.008	0.006	0.007	0.008	0.004	0.007	0.005	0.020	0.006	0.016	0.016
Mg	0.783	0.874	0.938	0.957	0.918	0.948	0.920	0.897	0.688	0.751	0.849	0.861	0.884	0.897	0.995	0.882	0.780	0.794	0.770	0.741
Ca	0.907	0.917	0.898	0.882	0.872	0.840	0.921	0.918	0.903	0.891	0.850	0.856	0.833	0.918	0.773	0.883	0.912	0.880	0.856	0.888
Na	0.020	0.019	0.011	0.011	0.016	0.015	0.015	0.015	0.025	0.027	0.024	0.024	0.020	0.015	0.014	0.025	0.024	0.019	0.035	0.037
Total	4.02	4.02	3.99	3.99	3.99	3.99	4.01	4.01	4.00	4.00	4.01	4.02	4.02	4.08	4.00	4.02	4.01	4.02	4.02	4.02
Mg#	78.7	86.8	87.7	88.0	85.1	85.0	90.0	87.6	72.1	72.8	80.0	80.3	78.4	81.9	84.5	85.2	75.2	78.2	72.0	72.0
En	41.1	45.3	48.3	49.4	47.7	49.1	47.3	46.1	38.8	39.8	47.9	50.8	50.0	47.2	50.8	45.9	39.6	41.8	44.9	43.3
Fs	11.3	7.1	7.0	6.9	8.8	9.0	5.4	6.7	15.5	15.4	10.5	8.7	10.0	9.5	9.7	8.2	14.1	11.9	13.5	13.3
Wo	47.6	47.6	44.7	43.7	43.5	41.9	47.3	47.2	45.7	44.9	41.6	40.5	40.0	43.3	39.5	45.9	46.3	46.3	41.5	43.4

Table 3. Representative microprobe analyses of orthopyroxene phenocrysts and microphenocrysts in volcanic rocks of western Anatolia.

Orthopyroxene														
Sample no. (c)ore/(r)im	EA45		EA412		EA412		EA418		EA37		EA313		EA275	
	c	r	c	r	c	r	c	r	c	r	c	r	c	r
SiO_2	52.81	52.87	52.55	52.88	52.12	52.20	52.04	53.19	51.32	51.98	54.91	51.98	52.60	52.68
TiO_2	0.35	0.33	0.52	0.49	0.44	0.50	0.41	0.18	0.15	0.12	0.13	0.12	0.15	0.17
Al_2O_3	0.90	1.29	1.97	1.92	1.85	1.75	1.43	0.91	0.85	0.60	2.38	0.60	0.88	0.60
FeO	17.07	15.39	17.18	17.06	18.22	18.02	17.71	18.09	20.01	20.22	8.31	20.22	20.93	21.11
MnO	0.50	0.39	0.39	0.38	0.37	0.40	0.44	0.80	0.95	1.24	0.19	1.24	1.17	1.26
MgO	25.21	26.58	24.61	24.70	23.98	23.95	24.37	24.85	23.61	22.70	31.66	22.70	22.79	22.34
CaO	1.62	1.46	1.94	1.95	1.82	2.00	1.94	1.38	0.96	0.94	1.04	0.94	1.23	1.21
Na_2O	0.04	0.04	0.08	0.10	0.07	0.07	0.04	0.02	0.02	0.022	0.02	0.02	0.03	0.04
Total	98.50	98.35	99.25	99.48	98.86	98.88	98.38	99.43	97.86	97.82	98.64	97.82	99.78	99.40
Si	1.958	1.946	1.935	1.941	1.936	1.938	1.934	1.962	1.947	1.973	1.940	1.973	1.962	1.975
Ti	0.010	0.009	0.015	0.014	0.012	0.014	0.011	0.005	0.004	0.003	0.003	0.003	0.004	0.005
Al	0.039	0.056	0.086	0.083	0.081	0.077	0.063	0.040	0.038	0.027	0.099	0.027	0.039	0.026
Fe	0.529	0.474	0.529	0.524	0.566	0.560	0.545	0.558	0.635	0.642	0.246	0.642	0.653	0.662
Mn	0.016	0.012	0.012	0.012	0.012	0.013	0.014	0.025	0.030	0.040	0.006	0.040	0.037	0.040
Mg	1.393	1.459	1.351	1.351	1.328	1.325	1.350	1.367	1.335	1.284	1.668	1.284	1.268	1.248
Ca	0.064	0.057	0.076	0.077	0.072	0.079	0.077	0.055	0.039	0.038	0.039	0.038	0.049	0.049
Na	0.003	0.003	0.006	0.007	0.005	0.005	0.003	0.001	0.002	0.002	0.001	0.002	0.002	0.003
Total	4.01	4.02	4.01	4.01	4.01	4.01	4.00	4.01	4.02	4.01	4.00	4.01	4.01	4.01
Mg#	72.5	75.5	71.9	72.1	70.1	70.3	71.2	71.0	67.8	66.6	87.2	66.7	66.0	65.4
En	70.9	74.7	68.6	68.8	67.1	67.0	68.2	69.0	67.4	66.1	85.1	66.1	63.4	62.5
Fs	25.8	22.2	27.5	27.3	29.2	29.0	27.8	28.2	30.5	31.9	12.8	31.9	34.2	35.0
Wo	3.4	3.1	3.9	3.9	3.7	4.0	3.9	2.8	2.0	2.0	2.0	2.0	2.5	2.4

phenocrysts and microphenocrysts from the Early Miocene, highly porphyritic acidic-intermediate lavas of the southern area classify predominantly as edenite and partly edenitic hornblende, though few fall into the pargasitic hornblende and ferroan-pargasite fields. Amphiboles from the Middle Miocene andesitic rocks of the southern area and the Early Miocene porphyritic lavas of the northern area, however, are characterized by lower Si contents (<6.5 pfu), and classify mainly as pargasite or ferroan-pargasite.

The plots of $Al^{[IV]}$ against (Na + K) cations in the A site of amphibole phenocrysts also reveal two distinct compositional groups (shown as an inset in Figure 6). The trends of the studied samples are comparable to those shown by the experimental studies of Helz (1973), which demonstrated that amphibole compositions in general exhibit linear increases in $Al^{[IV]}$ and $(Na + K)_A$ with increasing crystallization temperatures. The significant compositional difference between the two trends can therefore be attributed to different crystallization temperatures. The existence of both edenitic and pargasitic amphibole in a single rock may further indicate that these rocks are composite products of more than one petrogenetic stage.

Olivine

Olivine occurs in some form in most of the calc-alkaline and shoshonitic rocks of Middle Miocene age along with some Early Miocene dykes. It is, however, a scarce phenocryst phase in the acidic-intermediate rocks of Early Miocene lavas. Olivine phenocrysts and microphenocrysts,

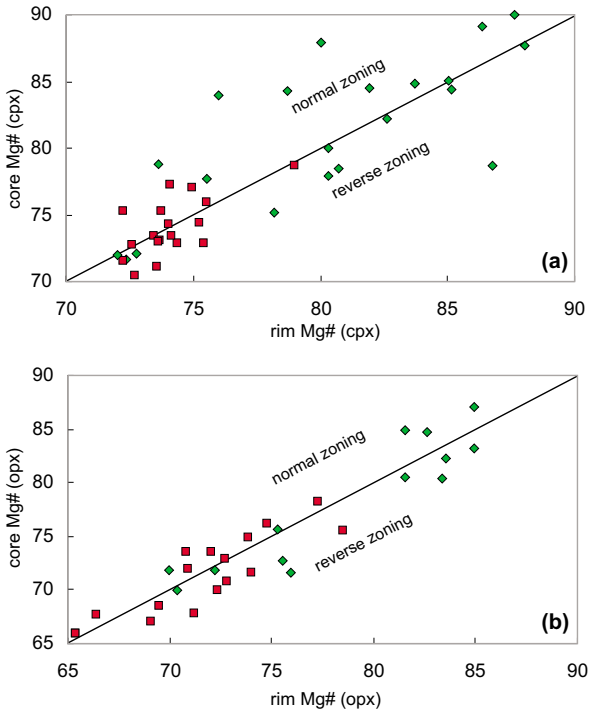

Figure 4. Core to rim variations in molar Mg# (100 – Mg / [Mg + Fe]) for the clinopyroxene and orthopyroxene phenocrysts. Volcanic rocks from the northern and southern areas are shown as squares and diamonds, respectively.

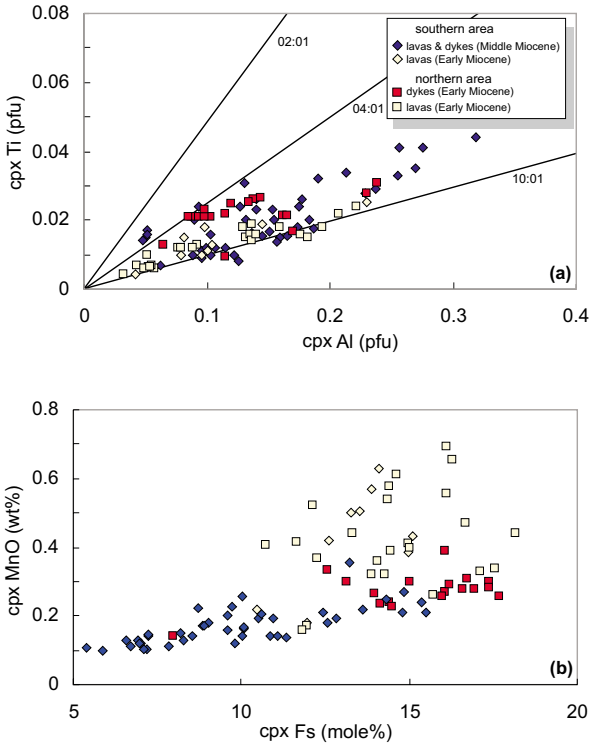

Figure 5. Minor element variations of clinopyroxenes shown by plots of **(a)** stoichiometric Ti versus Al (per formula unit); and **(b)** MnO contents versus the molar percentage of ferrosilite (Fs). Cores, rims and microphenocrysts do not plot in discrete fields and so are not distinguished. The lines in Figure **(a)** indicate Ti/Al ratios.

in general, show a compositional range of $Fo_{91\text{-}67}$ (Table 5). Mg contents of the olivines show only a small variation within the olivine-bearing rocks. Most of the phenocrysts have normal zoning, with a range of 5–15 mole %Fo. However, extreme variations from core to rim (Fo_{89} to Fo_{67}) are also observed in some samples.

Exchange coefficients (K_D values) calculated for distribution of Fe and Mg between olivine phenocrysts and liquids similar in composition to the host rocks $[(X_{FeO}/X_{MgO})_{ol}/(X_{FeO}/X_{MgO})_{liq}]$ (X = mole fraction) range between 0.24 and 0.31 for the common basaltic systems. Using the method of Roeder & Emslie (1970), Mg/Fe ratios of liquid with which the olivine compositions would have been in equilibrium were calculated and compared to Mg/Fe ratios of host rocks, to assess whether the olivines are in equilibrium with their host rocks. Figure 7 illustrates that, among the calc-alkaline and shoshonitic rocks of the Middle Miocene age, only few olivine crystals are within equilibrium range, but the majority are not. In particular, olivines from the intermediate rocks are too Fe-rich to have crystallized from a liquid compositionally similar to their host rocks. This can be explained either by mixing of magmas with different compositions or by accumulation of olivines as xenocrysts.

Biotite-Phlogopite

Biotite occurs as phenocrysts only in the highly porphyritic acidic-intermediate rocks (Early Miocene) of both the northern and southern areas. Some Middle Miocene shoshonitic rocks of the southern area include phlogopite as phenocrysts and as a dispersed groundmass phase. Compositions of biotite phenocrysts show no significant variations among different volcanic rock groups, nor within individual lava flows (Table 6), and they have constant Mg/Fe ratios (<2) and Al contents (>2.5 mole %). Phlogopite phenocrysts have

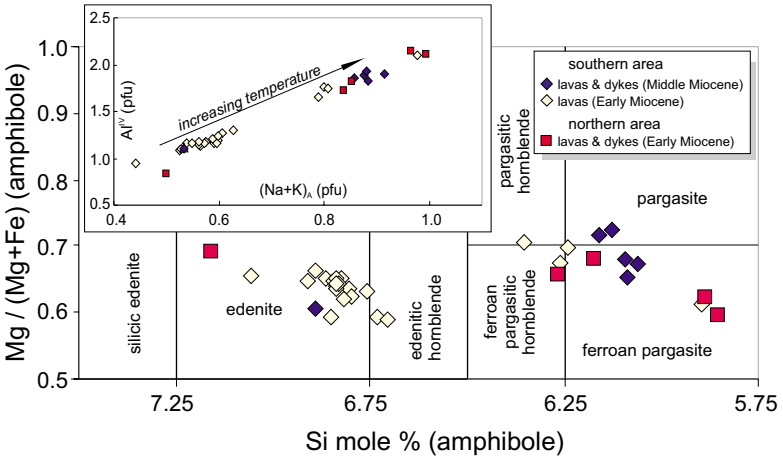

Figure 6. Amphibole phenocrysts plotted on the classification diagram of Hawthorne (1981). The inset diagram shows $Al^{[IV]}$ versus $(Na + K)_A$ site occupancy for amphibole phenocrysts. The inferred trend of increase in crystallization temperature is based on the experimental studies of Helz (1973).

Table 4. Representative microprobe analyses of amphibole phenocrysts and microphenocrysts in volcanic rocks of western Anatolia.

Amphibole														
Sample no. (c)ore/(r)im	EA147		EA99		EA364		EA326		EA316		EA112		EA273	
	c	r	c	r	c	r	c	r	c	r	c	r	c	r
SiO_2	45.52	45.36	44.45	45.47	38.42	47.23	45.72	44.99	45.16	45.28	39.83	39.99	41.00	40.69
TiO_2	1.50	1.57	1.35	1.27	2.64	1.07	1.46	1.66	1.49	1.51	2.85	2.38	3.42	2.88
Al_2O_3	7.46	7.57	8.31	7.44	13.52	6.13	7.61	8.04	7.84	7.76	12.83	12.64	11.04	11.85
FeO	13.14	13.20	15.61	15.48	13.46	13.47	13.39	13.99	14.24	14.37	11.25	12.11	11.72	11.24
MnO	0.38	0.41	0.44	0.41	0.19	0.43	0.39	0.39	0.43	0.44	0.15	0.21	0.15	0.14
MgO	13.79	13.90	12.53	12.73	11.86	14.31	13.97	13.44	13.32	13.14	13.14	12.94	12.62	13.45
CaO	11.43	11.46	11.75	11.68	11.94	11.74	11.53	11.52	11.54	11.46	11.66	11.76	11.43	11.55
Na_2O	1.48	1.55	1.52	1.39	1.96	1.13	1.46	1.51	1.47	1.44	2.16	2.22	2.14	2.19
K_2O	0.68	0.72	0.96	0.81	2.01	0.60	0.77	0.82	0.83	0.80	1.25	1.34	1.03	1.07
Total	95.41	95.77	96.95	96.77	96.05	96.15	96.33	96.38	96.32	96.19	95.16	95.60	94.61	95.17
Si	6.865	6.826	6.706	6.848	5.896	7.053	6.840	6.758	6.795	6.820	6.059	6.086	6.268	6.177
Ti	0.170	0.178	0.153	0.144	0.304	0.120	0.164	0.187	0.169	0.171	0.326	0.272	0.393	0.328
Al	1.326	1.342	1.478	1.321	2.445	1.079	1.341	1.423	1.390	1.377	2.301	2.267	1.989	2.120
Fe	1.657	1.661	1.970	1.949	1.727	1.683	1.675	1.758	1.791	1.810	1.431	1.541	1.498	1.427
Mn	0.048	0.053	0.056	0.053	0.024	0.054	0.050	0.049	0.055	0.056	0.020	0.027	0.019	0.018
Mg	3.101	3.117	2.818	2.857	2.713	3.186	3.116	3.010	2.987	2.951	2.981	2.935	2.877	3.044
Ca	1.847	1.847	1.899	1.885	1.964	1.878	1.848	1.855	1.860	1.849	1.901	1.917	1.873	1.879
Na	0.433	0.453	0.444	0.406	0.583	0.328	0.424	0.441	0.430	0.420	0.637	0.656	0.635	0.644
K	0.132	0.138	0.184	0.155	0.393	0.115	0.147	0.157	0.160	0.154	0.243	0.259	0.201	0.207
Total	15.58	15.62	15.71	15.62	16.05	15.50	15.61	15.64	15.64	15.61	15.90	15.96	15.75	15.84
Mg#	0.555	0.553	0.571	0.596	0.414	0.609	0.555	0.553	0.563	0.568	0.383	0.405	0.430	0.402

Table 5. Representative microprobe analyses of olivine phenocrysts and microphenocrysts in volcanic rocks of western Anatolia.

Olivine														
Sample no. (c)ore/(r)im	EA350		EA134		EA348		EA313		EA101		EA409		EA399	
	c	r	c	r	c	r	c	r	c	r	c	r	c	r
SiO_2	38.96	39.94	39.24	38.72	38.48	37.52	38.10	37.77	36.14	36.17	36.78	38.00	39.83	39.14
Fe_2O_3	13.29	8.93	14.24	15.74	17.23	20.28	21.86	23.72	28.00	28.63	23.52	21.30	10.42	14.40
MnO	0.23	0.15	0.32	0.35	0.32	0.39	0.44	0.48	0.63	0.63	0.49	0.37	0.20	0.26
MgO	46.48	50.21	44.71	44.32	43.21	40.75	39.44	37.77	34.03	33.47	36.44	38.81	48.72	45.16
CaO	0.17	0.20	0.20	0.19	0.12	0.17	0.12	0.13	0.35	0.37	0.26	0.30	0.32	0.35
Total	99.13	99.43	98.70	99.31	99.36	99.11	99.95	99.86	99.15	99.27	97.50	98.78	99.49	99.31
Si	0.97	0.98	1.00	0.98	0.98	0.97	0.99	0.99	0.98	0.98	0.99	1.00	0.98	0.99
Fe	0.27	0.18	0.30	0.33	0.36	0.43	0.47	0.52	0.63	0.64	0.53	0.47	0.21	0.30
Mn	0.01	0.00	0.01	0.01	0.01	0.01	0.01	0.01	0.01	0.02	0.01	0.01	0.00	0.01
Mg	1.73	1.83	1.69	1.68	1.64	1.57	1.53	1.48	1.37	1.35	1.46	1.52	1.79	1.70
Ca	0.01	0.01	0.01	0.01	0.00	0.01	0.00	0.00	0.01	0.01	0.01	0.01	0.01	0.01
Total	3.00	3.00	3.00	3.02	3.00	3.00	3.01	3.01	3.00	3.00	3.01	3.00	3.00	3.00
Fo	86.43	91.21	84.84	83.39	81.92	78.39	76.28	73.94	68.61	67.75	73.42	76.46	89.49	84.96
Fa	13.57	8.79	15.16	16.61	18.08	21.61	23.72	26.06	31.39	32.25	26.58	23.54	10.51	15.04

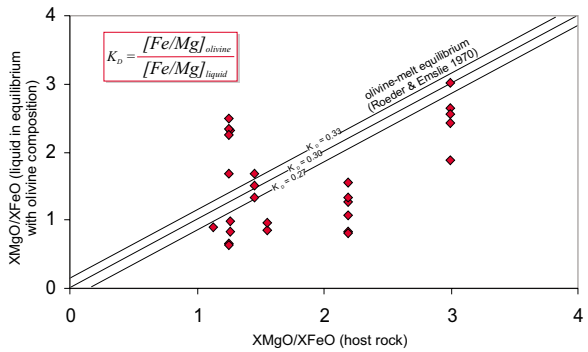

Figure 7. Equilibrium X_{MgO}/X_{FeO} ratio of liquid calculated from olivine compositions plotted against X_{MgO}/X_{FeO} ratio of host rock for the Middle Miocene volcanic rocks of western Anatolia (X is mole fraction of oxide). Lines represent equilibrium between minerals and bulk rock compositions. Equilibrium range was calculated using equilibrium $^{Fe/Mg}K_{Dmin/liq}$ values from Roeder & Emslie (1970). The olivine compositions, in general, are not in Mg–Fe exchange equilibrium with the melt compositions of the host lavas at a K_D value of 0.30±0.03. They are therefore believed to have either formed as accumulated xenocrysts or crystallized from relatively evolved magmas.

characteristically higher Mg/Fe ratios (>2.5) and lower Al contents (<2.3 mole %) than biotites. Ti contents are unusually high for all phlogopites.

Fe-Ti Oxides

All samples from the western Anatolian volcanic suites contain Ti-rich magnetite (Fe_3O_4 – Fe_2TiO_4; titaniferous magnetite), whereas ilmenite is only present in the dykes of both areas. Magnetites (or titanomagnetite) are subhedral to anhedral in shape, range from 0.1–0.5 mm in diameter, and are in many cases adjacent to plagioclase or pyroxene phenocrysts; groundmass magnetite is present as scattered, typically euhedral crystals <0.1 mm in size. Magnetite comprises 2 to 3 vol% of phenocrysts. Ilmenite, where present, is much less abundant than magnetite. It is characteristically associated with magnetite or found as inclusions in pyroxene. The low modal abundance of ilmenite is typical of arc-related or continental calc-alkaline magmatic suites and is likely to result from the low Ti contents of magmas.

Table 6. Representative microprobe analyses of biotite/phlogopite phenocrysts and microphenocrysts in volcanic rocks of western Anatolia.

Biotite / Phlogopite								
Sample no.	EA109	EA350	EA134	EA316	EA147	EA37	EA231	EA73
SiO_2	38.64	38.95	38.98	36.18	36.23	36.30	34.97	35.21
TiO_2	5.45	7.12	6.40	4.55	5.17	4.74	5.48	4.68
Al_2O_3	12.92	12.89	12.12	13.45	13.30	13.72	14.60	14.42
Fe_2O_3	9.37	7.91	7.28	15.90	14.13	15.82	14.54	14.80
MnO	0.13	0.06	0.09	0.23	0.14	0.24	0.15	0.24
MgO	16.61	19.11	19.18	14.13	15.20	14.05	14.36	14.69
Na_2O	0.69	0.47	0.78	0.50	0.59	0.51	0.61	0.67
K_2O	8.86	9.41	8.73	8.29	8.59	8.43	8.71	8.56
Total	93.02	96.20	93.55	93.23	93.35	93.79	93.52	93.36
Si	5.75	5.59	5.97	5.80	5.77	5.79	5.33	5.38
Ti	0.61	0.77	0.74	0.55	0.62	0.57	0.63	0.54
Al	2.27	2.18	2.19	2.54	2.50	2.58	2.62	2.60
Fe	1.17	0.95	0.93	2.13	1.88	2.11	1.85	1.89
Mn	0.02	0.01	0.01	0.03	0.02	0.03	0.02	0.03
Mg	3.69	4.09	4.38	3.38	3.61	3.34	3.26	3.34
Na	0.20	0.13	0.23	0.15	0.18	0.16	0.18	0.20
K	1.68	1.72	1.71	1.70	1.75	1.71	1.69	1.67
	15.38	15.43	16.16	16.29	16.32	16.29	15.58	15.64
Mg/Fe	3.16	4.31	4.70	1.58	1.92	1.58	1.76	1.77

The chemical compositions of these oxide phases are reported in Table 7. The Fe^{3+} in the oxide minerals is estimated from the difference between Ti and Fe plus other divalent cations. Compositions of titanomagnetites are close to binary solid-solution series of magnetite-ulvospinel. Titanomagnetite has an ulvospinel molar fraction that varies from 16 to 45%, whereas ilmenite-hematite solid solution has an ilmenite molar fraction varying from 80 to 87%.

Magmatic Intensive Parameters

Estimates of Pre-eruptive Temperature and Oxygen Fugacity

Pyroxene Thermometry. Electron-microprobe data of pyroxenes from the western Anatolian lavas were used to calculate Wo-En-Fs end-members according to the projection scheme of Lindsley & Andersen (1983). The amount of Fe^{3+} in clinopyroxenes was calculated by mass balance (Lindsley 1983), and found to be minimal. Compositions of coexisting clinopyroxene and orthopyroxene with less than 10% non-quadrilateral components were plotted onto the quadrilateral with isotherms proposed by Lindsley (1983) to estimate temperatures (Figure 8). The temperature of coexisting clinopyroxenes and orthopyroxenes was also calculated for comparison using the QUILF program of Andersen *et al.* (1993), and obtained similar results to those of quadrilateral projection calibrated for 1 atmosphere pressure (Table 8). Although crystallization pressures may vary significantly for the western Anatolian lavas, the use of 1 atm diagram would have no significant effect on temperature estimates as there is only a slight difference between the contours of the diagrams calibrated for 1 atm and 10 kb unless the temperature is higher than 1100 ºC (e.g., Lindsley 1983). Pyroxene thermometry was applied to pyroxene phenocrysts from most of the Early–Middle Miocene calc-alkaline and shoshonitic lavas.

The estimated pyroxene temperatures for different volcanic units of western Anatolia are presented in Figure 8 and Table 8. Coexisting clinopyroxene and orthopyroxene phenocrysts from the volcanic rocks of the northern area have similar crystallization temperatures

Table 7. Microprobe analyses of coexisting magnetite and ilmenite in volcanic rocks of western Anatolia.

Oxides																		
Sample no.	EA350		EA348		EA399		EA409		EA112		EA101		EA231		EA45		EA418	
	mag	ilm	mag	ilm	mag	ilm	mag	ilm	mag	ilm	mag	ilm	mag	ilm	mag	ilm	mag	ilm
SiO_2	0.10	0.14	0.04	0.11	0.12	0.08	0.10	0.11	0.06	0.13	0.06	0.09	0.17	0.22	0.18	0.48	0.08	0.10
TiO_2	12.04	40.41	8.99	44.50	5.10	43.86	4.94	42.05	12.20	48.00	13.79	47.22	10.52	42.87	14.02	34.20	8.51	36.03
Al_2O_3	2.78	1.13	2.04	0.18	0.95	0.07	1.91	0.11	2.84	0.19	3.15	0.14	3.37	0.11	2.21	0.48	2.34	0.85
Fe_2O_3	44.46	26.57	42.36	18.63	58.13	17.95	58.25	20.84	42.91	12.08	38.27	13.80	45.13	16.99	37.66	36.15	51.06	39.16
FeO	34.48	24.44	36.03	31.38	34.40	34.81	34.33	33.43	37.27	31.71	37.89	31.57	38.11	33.04	40.92	25.79	36.02	10.27
MnO	0.59	0.69	0.41	0.51	0.14	0.61	0.17	0.39	0.62	0.71	0.60	0.57	0.75	1.78	0.80	1.41	0.32	1.04
MgO	3.43	5.68	2.17	3.88	0.67	2.19	0.89	2.12	3.17	5.86	4.07	5.66	1.78	1.86	1.30	1.57	1.62	11.66
Cr_2O_3	1.10	0.17	8.68	0.13	0.32	0.18	0.23	0.17	0.63	0.08	3.08	0.15	0.12	0.03	0.08	0.05	0.09	0.21
Total	98.97	99.23	100.72	99.33	99.82	99.75	100.82	99.22	99.70	98.76	100.91	99.20	99.95	96.90	97.17	100.13	100.04	99.32
Si	0.004	0.003	0.001	0.003	0.004	0.002	0.004	0.003	0.002	0.003	0.002	0.002	0.006	0.006	0.007	0.012	0.003	0.002
Ti	0.323	0.729	0.243	0.821	0.142	0.825	0.136	0.796	0.336	0.898	0.372	0.866	0.292	0.827	0.402	0.641	0.236	0.610
Al	0.117	0.032	0.087	0.005	0.042	0.002	0.082	0.003	0.122	0.006	0.133	0.004	0.146	0.003	0.099	0.014	0.102	0.023
Fe^{+3}	1.194	0.497	1.175	0.344	1.652	0.338	1.629	0.394	1.182	0.189	1.031	0.253	1.253	0.328	1.080	0.678	1.416	0.748
Fe^{+2}	1.029	0.510	1.115	0.664	1.099	0.728	1.079	0.703	1.141	0.660	1.135	0.644	1.175	0.709	1.304	0.558	1.110	0.193
Mn	0.018	0.014	0.013	0.011	0.004	0.013	0.005	0.008	0.019	0.015	0.018	0.012	0.023	0.039	0.026	0.030	0.010	0.020
Mg	0.183	0.203	0.116	0.142	0.037	0.082	0.048	0.079	0.173	0.217	0.217	0.206	0.098	0.071	0.074	0.058	0.089	0.391
Cr	0.031	0.003	0.247	0.003	0.009	0.004	0.007	0.003	0.018	0.002	0.087	0.003	0.003	0.001	0.002	0.001	0.003	0.004
Total	3.00	2.00	3.00	2.00	3.00	2.00	3.00	2.00	3.00	2.00	3.00	2.00	3.00	2.00	3.00	2.00	3.00	2.00

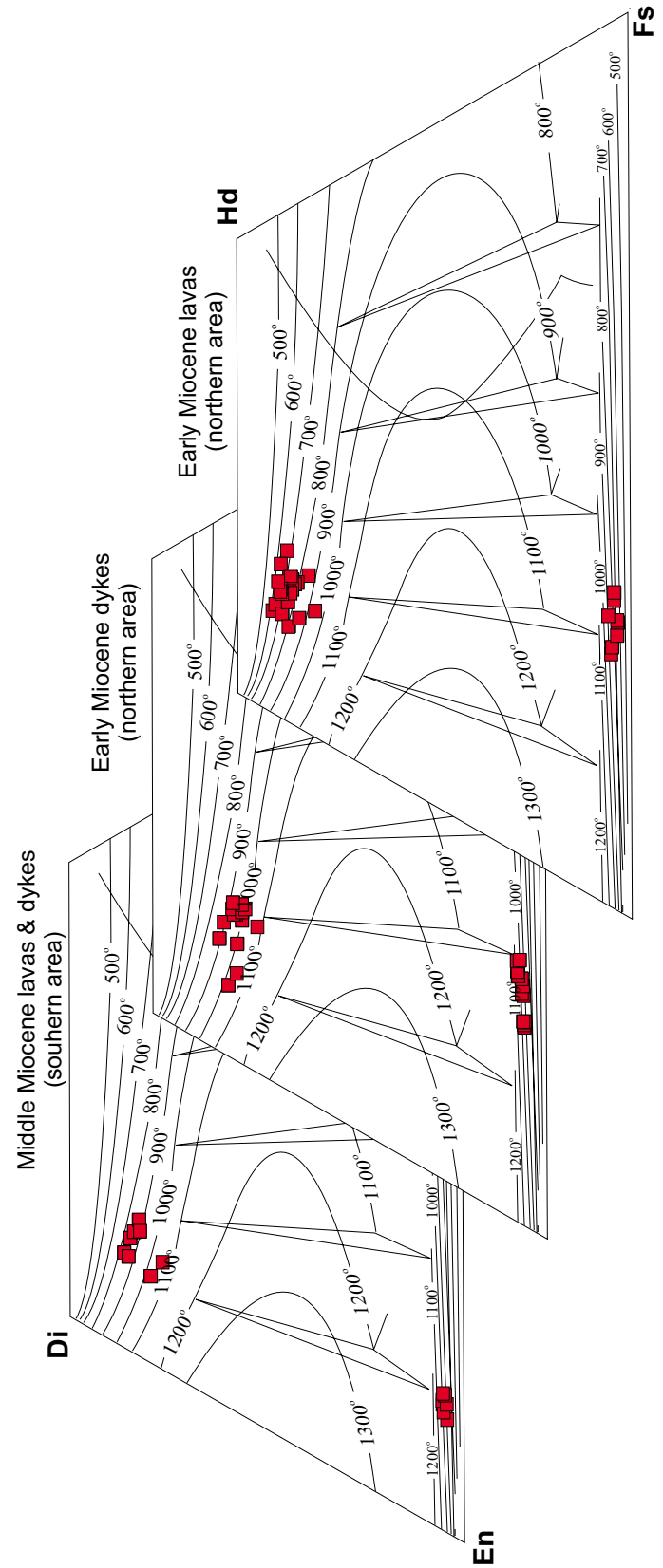

Figure 8. Pyroxene quadrilateral with data points representing the compositions of cores (white) and rims (grey) of pyroxenes of western Anatolian volcanic rocks. Correction methods for Na and Al and 1 bar isotherms are after Lindsley & Andersen (1983). The liquidus temperatures of pyroxenes plotted on the Di-En-Hd-Fs quadrilateral of Lindsley (1983); calibrated to 1 atmosphere pressure and contoured at 100 °C intervals.

Table 8. Calculated temperatures and pressures of crystallization and oxygen fugacity of the melts.

Area	Age	Sample locality	Flow type	Sample no.	Rock type	T (°C)[a]	T (°C)[b]	T (°C)[c]	P (kbar)[d]	P (kbar)[e]	LogfO_2
Northern Area	Early Miocene	Assos	lava (porph.)	EA37	trac-and	783					
		Assos	lava (porph.)	EA275	trac-and	847					
		Assos	lava (porph.)	EA78	trac-and	965			5.6		
		Assos	lava (porph.)	EA73	trac-and	785	860			8.8	
		Ayvacık	lava (porph.)	EA273	trac-and	812	918			6.7	
		Ayvacık	lava (porph.)	EA231	trac-and	724		866			-11.9
		Gülpınar	lava (porph.)	EA67	trac-dac	585					
		Gülpınar	lava (porph.)	EA62	trac-and	673					
		Babakale	dyke	EA45	trac-and	1047		1045	4.8		-8.8
		Babakale	dyke	EA412	trac-and	1086					
		Babakale	dyke	EA418	bas-trac-and	914		917	5.2		-10.2
Southern Area	Early Miocene	Bergama	lava (porph.)	EA316	dac		792			7.1 - 4.2	
		Ayvalık	lava (porph.)	EA147	dac		790			3.4	
		Dikili	lava (porph.)	EA99	trac-and		836			3.6	
		Mt. Seyret (summit)	lava (porph.)	EA364	trac-and		768			8.6 - 2.1	
		Mt. Seyret (flank)	lava (porph.)	EA326	trac-dac		850			3.4	
	Middle Miocene	Bergama	lava (aphyric)	EA313	and	1095			8.1		
		Nebiler	lava (aphyric)	EA109	bas-trac-and						
		Nebiler	lava (aphyric)	EA134	bas-trac-and				7.2		
		Nebiler	lava (aphyric)	EA143	bas-and	820			6.5		
		Nebiler	dyke	EA348	bas-and			851			-12.0
		Nebiler	dyke	EA350	bas-trac-and	914		938			-10.5
		Dikili	dyke	EA101	bas-trac-and			880	9.1		-12.2
		Dikili	dyke	EA112	and			807		6.8	-13.9
		Foça	dyke	EA399	trac-bas			785			-12.9
		Foça	dyke	EA409	trac-bas			794	7.4		-12.5

[a] Two-pyroxene thermometer of Lindsley (1983).
[b] Amphibole-plagioclase thermometer of Blundy & Holland (1994).
[c,f] Oxide thermobarometry. Calculations were using with the ILMAT program of LePage (2003) using the solution models of Andersen & Lindsley (1988).
[d] Clinopyroxene barometer of Putirka *et al.* (2003).
[e] Al-in-hornblende barometer of Schmidt (1992).

indicating they are equilibrium assemblages (Figure 8). A remarkable difference, however, can be seen between the crystallization temperatures of pyroxenes from the porphyritic lavas and those from the dyke swarms among the volcanic rocks of the northern area. Pyroxenes of the porphyritic lavas typically have lower crystallization temperatures relative to those of the dyke swarms; the estimated temperatures range from 585 to 965 ºC for the lavas and from 914 to 1086 ºC for the dykes (Table 8). The estimated temperatures for pyroxenes of the Middle Miocene lavas of the southern area are generally high (>820 ºC).

Phenocryst cores in most of the samples from the Early Miocene lavas yield higher temperatures than their rims. In some of the samples, however, Ca-poor rims of reversely zoned clinopyroxene phenocrysts yield temperature estimates 5 to 50 ºC higher than their cores. This feature may suggest that – throughout the formation of the volcanic suites – the magma chambers were periodically heated up, probably through recharge of hotter magma to the base.

Amphibole-Plagioclase Thermometer. Electron-microprobe data for the amphibole and plagioclase phenocrysts from the western Anatolian volcanic rocks were used to estimate temperature using the equations proposed by Holland & Blundy (1994). The use of this thermometer can only be applied to the amphibole-bearing, acidic-intermediate rocks of the southern area because of the scarcity of amphibole as an equilibrium assemblage in most other volcanic units of the area. The calculations were made using plagioclase rim compositions because these are thought to most likely represent the compositions in exchange equilibrium with the coexisting amphiboles. The uncertainty in the thermometer is considered to be ±40 ºC (Holland & Blundy 1994). Solid pressures for the mineral assemblages used in the temperature calculations were estimated using Schmidt's (1992) Al-in-hornblende method.

The results obtained from the amphibole-plagioclase thermometer are given in Table 8. The temperatures estimated for the porphyritic lavas (*samples EA273 and EA231*) of the northern area are in the range of 860–918 ºC, which is notably higher than estimates obtained from pyroxene thermometry (Table 8); this may be a result of the fact that amphiboles in this suite are not in equilibrium with melt and, hence, amphibole and plagioclase phenocrysts may not coexist. These results of temperature estimates should therefore be interpreted with caution, as they may not represent crystallization temperatures. On the other hand, estimates from amphibole phenocrysts yield a temperature range of 768–850 ºC for the Early Miocene, acidic-intermediate rocks of the southern area. The results also show that the estimated temperatures of crystallization decrease with increasing silica content of the host rocks, strongly suggesting the influence of magma composition on crystallization temperatures.

Fe-Ti Oxide Thermometry and Oxygen Fugacity. Estimation of temperatures and oxygen fugacity (fO_2) at the time of crystallization were attempted using the equilibria between two solid solutions with thermodynamic analysis of Fe-Mg-Ti oxides calibrated by Andersen & Lindsley (1988). Only samples that were likely to have preserved equilibrium conditions, as determined from Mg and Mn partitioning (e.g., Bacon & Hirschmann 1988), were used to calculate temperatures. Ilmenite does not occur with titanomagnetite in most of the lavas of the western Anatolian suite, preventing utilization of two oxide phases for estimating temperature and fO_2. Temperature and fO_2 estimates using Fe-Ti oxides were therefore restricted only to the dyke rocks of both areas, as well as to some Early Miocene rocks of the northern area. Magnetite–ilmenite geothermometry calculations were carried out on the western Anatolian samples using the ILMAT program of LePage (2003), with temperatures and fO_2 calculated for the solution model of Andersen & Lindsley (1988).

Although some of the results obtained carry major uncertainties due to significant quantities of minor elements (e.g., Al, Mg) and within-sample variations in oxide compositions, only temperature estimates with uncertainties of less than 50 ºC were used (Table 8). The temperature estimates range from 785 to 938 ºC for the Middle Miocene rocks of the southern area and from 866 to 1045 ºC for Early Miocene rocks of the northern area. The latter range seems to be consistent with that obtained by pyroxene thermometry (Table 8). Oxygen-fugacity values obtained from the dykes of both areas fall above the QMF buffer curve, indicating moderately oxidizing conditions (Figure 9). A decrease in oxygen

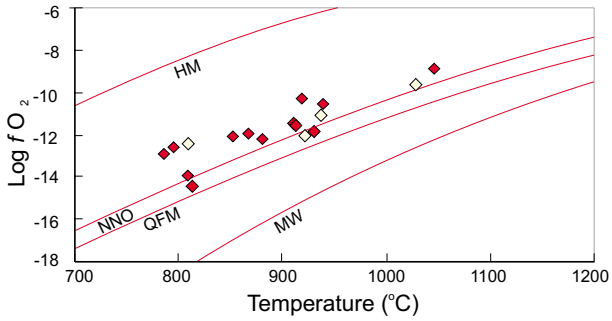

Figure 9. Temperature (T) and oxygen fugacity (fO_2) conditions calculated from the composition of coexisting cubic (titanomagnetite) and rhombohedral (ilmenite) solid solutions. Curves define solid oxygen buffers corresponding to hematite-magnetite (HM; Myers & Eugster 1983); quartz-fayalite-magnetite (QFM; Berman 1988); magnetite-wüstite (MW; Myers & Eugster 1983); and nickel-nickel oxide (NNO; Heubner & Sato 1970). Open and closed diamonds represent dykes from the northern and southern areas, respectively.

fugacity with falling temperature is also indicated for the dykes from both areas.

Pressure of Crystallization

Clinopyroxene Geobarometer. Electron-microprobe data for clinopyroxene phenocrysts from the least differentiated samples among the western Anatolian volcanic rocks were used to estimate pressure of crystallization, according to the clinopyroxene geobarometer of Putirka *et al.* (2003). A number of preliminary steps, however, are required before calculating the pressures of crystallization. These include: (1) calculation of cation fractions from whole-rock major-element analyses; (2) calculation of DiHd (diopside + hedenbergite), EnFs (enstatite + ferrosilite), and the sum of the total components (definitions in Putirka *et al.* 2003) for the analyzed clinopyroxenes; (3) calculation of the DiHd, EnFs and sum parameters for model clinopyroxenes in equilibrium with liquids having the same chemical composition as the samples; and (4) comparison of these values with the DiHd, EnFs and sum components of the measured pyroxenes. Because no glass is present in the rocks that could be analyzed by electron microprobe, no measured liquid compositions were available. We have, therefore, applied fractionation correction to estimate the composition of the liquids from which each of the rock samples used in this application are likely to have originated.

The results of pressure estimates from pyroxene phenocrysts are given in Table 8. Pyroxenes from the Middle Miocene basic-intermediate rocks of the southern area characteristically yield pressure estimates that range between 6.5–9.1 kbar (with the majority >7 kbar). Pressure estimates of clinopyroxenes from the Early Miocene volcanic rocks of the northern area range between 4.8 and 5.6 kbar and are generally lower than those obtained from the Middle Miocene mafic-intermediate rocks.

Al-in-Hornblende Geobarometer. Electron-microprobe data from amphibole phenocrysts in the Early Miocene intermediate rocks of the southern area were used for estimating pressure, applying the Schmidt (1992) Al-in-hornblende barometer. The results are given in Table 8. Analyzed amphibole phenocrysts from the porphyritic lavas of the southern area generally yield similar pressure estimates. These estimates generally range between 2 and 4 kbar and indicate low-pressure fractionation. In some of the samples, however, two different ranges of pressure estimates were obtained: one range between 2.1–4.2 kbar, and the other between 7.1–8.6 kbar. This may be explained by more than one stage of amphibole crystallization in magma chambers at different depths.

Disequilibrium Parameters

During magma storage and ascent, changes in melt composition occur due to fractional crystallization or magma mixing, and changes in the physical conditions of crystallization occur due to cooling, decompression or magma mixing. Mixing may take place between distinct magma batches or between different zones of the same magma chamber through a convective self-mixing process (e.g., Couch *et al.* 2001). The signatures of all these processes might be recorded in the compositional and textural zoning of phenocrysts (e.g., Hibbard 1981; Davidson *et al.* 1998; Ginibre *et al.* 2002; Troll & Schmincke 2002).

Compositional and textural characteristics of the rocks under consideration show that the most important petrographic features of the Early Miocene, acidic-intermediate rocks of western Anatolia are their high phenocryst contents (up to 65%) and the complex compositional zoning of their plagioclase and pyroxene phenocrysts. Such textures and chemical-zoning patterns

of phenocrysts suggest that parts of the mineral assemblage were not in equilibrium with one another (and with the melt) prior to or during the eruption of magma batches. Phenocrysts with disequilibrium crystal textures and microphenocrysts make up more than 60 vol% of the total crystal population. Other evidence for disequilibrium includes reaction rims on scarce amphibole crystals, and reaction corona textures in most of the plagioclase phenocrysts.

Plagioclase phenocrysts in most of the western Anatolian volcanic rocks also show clear evidence of multiple origins and periods of dissolution and growth. Complex compositional zoning, common in calc-alkaline volcanic rocks, is seen in conjunction with sieve texture in zones of and dissolution surfaces on phenocrysts. Although there are samples with "unsieved" and unzoned plagioclase, most of the lavas contain phenocrysts with disequilibrium features. These phenocrysts exhibit cores that are partly resorbed, resulting in honeycomb, or sieve texture. The sieve texture consists of crystal patches (0.30–1.0 mm) separated by similarly sized runnels of brown glass. Melt channels cut both twin planes in single crystals and crystal faces in glomerocrysts. The resorbed cores are typically anhedral, and where in contact with melt, possess overgrowths forming euhedral phases.

Complex compositional zoning of crystals is mostly attributed to magma-mixing processes (e.g., Dungan & Rhodes 1978; Tsuchiyama 1985; Nixon & Pearce 1987; Davidson *et al.* 1998; Tepley *et al.* 2000). For plagioclase, normal compositional zoning, characterized by more calcic core compositions relative to rim compositions, can be explained by increasing the degree of crystallinity within a sample. However, reverse zoning that is accompanied by normal zoning in crystals within the same sample can most easily be explained by magma mixing (or contamination by wall rock). In mixing systems, a more sodic crystal, derived from a felsic magma component, will tend to be resorbed as it is reheated by the more mafic magma component. This may give rise subsequent crystallization of more calcic plagioclase in the outer zones of phenocrysts. If calcic crystals of the mafic component happen to be present at the time of mixing, they will not be resorbed and will retain well-developed crystal shapes and will be mainly enclosed by further growth zones. Overgrowths of these mixing plagioclase crystals are mostly dusty and characterized by dendritic texture resulting from quenching of relatively calcic plagioclase melt of the mafic component. In some cases, nucleation of plagioclase dendrites may comprise a dendritic core of a crystal that has an overgrown rim of later-formed non-dendritic plagioclase. In some other cases, repetitive injection of mafic magma into a relatively less mafic magma chamber may form oscillatory zoned phenocrysts which are marked by multiple resorption cycles, producing resorbed and sieve-textured crystals, although some argue that formation of sieve-textured plagioclase may be attributed to rapid magmatic decompression rather than to mixing (e.g., Nelson & Montana 1992).

Most plagioclase phenocrysts of the highly porphyritic, Early Miocene acidic-intermediate rocks of the western Anatolian suites display most of the textural features described above. These mineralogical and textural characteristics of the plagioclase phenocrysts may indicate that the lavas in these suites have experienced extensive, open-system differentiation. The highly porphyritic nature of most of these lavas may further suggest that open-system modification might have been operational in shallow-level magma chambers.

It is evident from the low phenocryst contents (<3–30%) of the Middle Miocene basic-intermediate rocks that the degree of crystallinity decreases gradually over time, from the Early Miocene to the Middle Miocene. Unlike the Early Miocene rocks, the aphyric or weakly porphyritic nature of the rocks of Middle Miocene age may indicate that the magmas have not experienced long-lived, shallow-level magma-chamber processes; this possibly reflects a rapid ascent of the magmas through crustal conduit systems as a consequence of progressive thinning and fracturing of the crust – probably in association with more pronounced regional extensional tectonics.

Model for Magma-Chamber Processes

Water has a profound effect on melt dynamics in arc- and collision-related continental settings, and controls processes such as mixing, assimilation and differentiation (Gaetani *et al.* 1993; Sisson & Grove 1993; Hort 1998; Barclay & Carmichael 2004), as well as the eruptive behaviour of magmas on the Earth's surface (e.g., Sparks *et al.* 1994; Bower & Woods 1997). The volcanological and petrographic characteristics of the rocks of this study show that water plays an important role in the genesis of

the western Anatolian calc-alkaline and shoshonitic series. These include common explosive magmatic products, development of highly vesicular products (e.g., existence of pumice flows), eruption of phenocryst-rich magmas with dramatic compositional zoning of phenocrysts, and frequent crystallization and preservation of hydrous mineral phases (even in basaltic compositions). Petrographic characteristics of the volcanic rocks may further indicate that crystallization of amphibole in the genesis of the calc-alkaline and shoshonitic lavas may have been of particular importance.

A number of experimental studies were conducted on water-saturated, basaltic and andesitic systems to define the possible role of amphibole crystallization (with other mineral assemblages) on magma genesis in island-arc and continental environments. Some of these experiments have shown that amphibole is a liquid phase in basaltic to basaltic-andesitic magmas under near water-saturated conditions (>10% H_2O) and pressures of 8 to 25 kbar (e.g., Gill 1981; Green 1982). In another study, Foden & Green (1992) conducted experiments on high-Al basalt system with H_2O under melting pressures between 1 atm and 10 kbar to define the amphibole stability field and the composition of the liquids coexisting with amphibole. Those authors proposed a model whereby basaltic-andesite melt may be generated either through interaction of hydrous mafic melts with peridotitic wall rock or by melting of an amphibole-peridotite source. They also suggested a phase diagram for the high-Al basalt system with ~5% H_2O illustrating possible cooling paths and crystallization products at different stages. In Figure 10, the phase diagram of Foden & Green (1992) is given together with a schematic illustration of the petrological model inferred by this study, which is based on the mineral-disequilibrium data presented here. The model proposed for the rocks under consideration displays the general framework for the plumbing system in the thickened continental crust beneath western Anatolia. The approximate depth of the proposed magma chambers are estimated using crystallization pressures.

The crystallization-pressure calculations and petrographic characteristics show that the volcanic rocks of the northern area have a polybaric origin and are the composite products of more than one petrogenetic step. This is evident from strong compositional variations within single phenocrysts, as well as from considerably variable crystallization pressures. The rocks in this suite generally have large proportions of phenocrysts crystallized at pressures between ~4 (constrained by the crystallization of biotite; e.g., Naney 1983) and 5.6 kbar, corresponding to a crystallization depth of 12 to 20 km. These are mainly plagioclase-, pyroxene- and magnetite-bearing assemblages. Amphibole crystals of pargasitic composition in some of the rocks, however, yield higher pressures (Table 8), implying that the early crystallization of the magma took place at depths of about 30 km, near the crust-mantle transition.

The compositions of amphiboles that Foden & Green (1992) synthesized in their experiments were mainly pargasitic hornblende. Their results showed that plagioclase is the anhydrous liquidus phase between 1 atm and 10 kbar, but in the hydrous environments its role is taken by olivine at pressures greater than 7 kbar, and then by clinopyroxene at more elevated pressures. Amphibole of pargasitic hornblende composition may crystallize in magmatic systems if a magma body, as a whole, remains motionless over a period of time and experiences extensive convection and mixing (in the sense of closed-system equilibrium crystallization); or if the wall-rock with which cooling, hydrous basaltic melts are in contact (in the sense of open magmatic system), is composed of olivine and pyroxene, as in the case of the upper mantle or lower crust (point C in Figure 10).

The amphiboles found in the rocks of the northern area are mainly pargasitic (or ferroan pargasitic) hornblende that yield high-pressure crystallization conditions. This may imply that the primary magmas initially ponded in deep crustal reservoirs (~30 km) where they underwent combined fractional crystallization and crustal assimilation, or mixed with crustal melts. Processes that affected the primary magma compositions in deep crustal reservoirs may be regarded as open-system processes, in a manner similar to the MASH (melting, assimilation, storage and homogenization) hypothesis proposed by Hildreth & Moorbath (1988). The early fractionation in deep magma chambers is likely to have performed the function of re-establishing buoyant ascent of magma to form higher level magma chambers having variable depths, sizes and fractionating assemblages.

In the deep magma chambers, if liquid tapped and extracted from crystalline matrix, the crystallizing phases will move back into the field of olivine and clinopyroxene (with or without plagioclase) as the adiabatic temperature

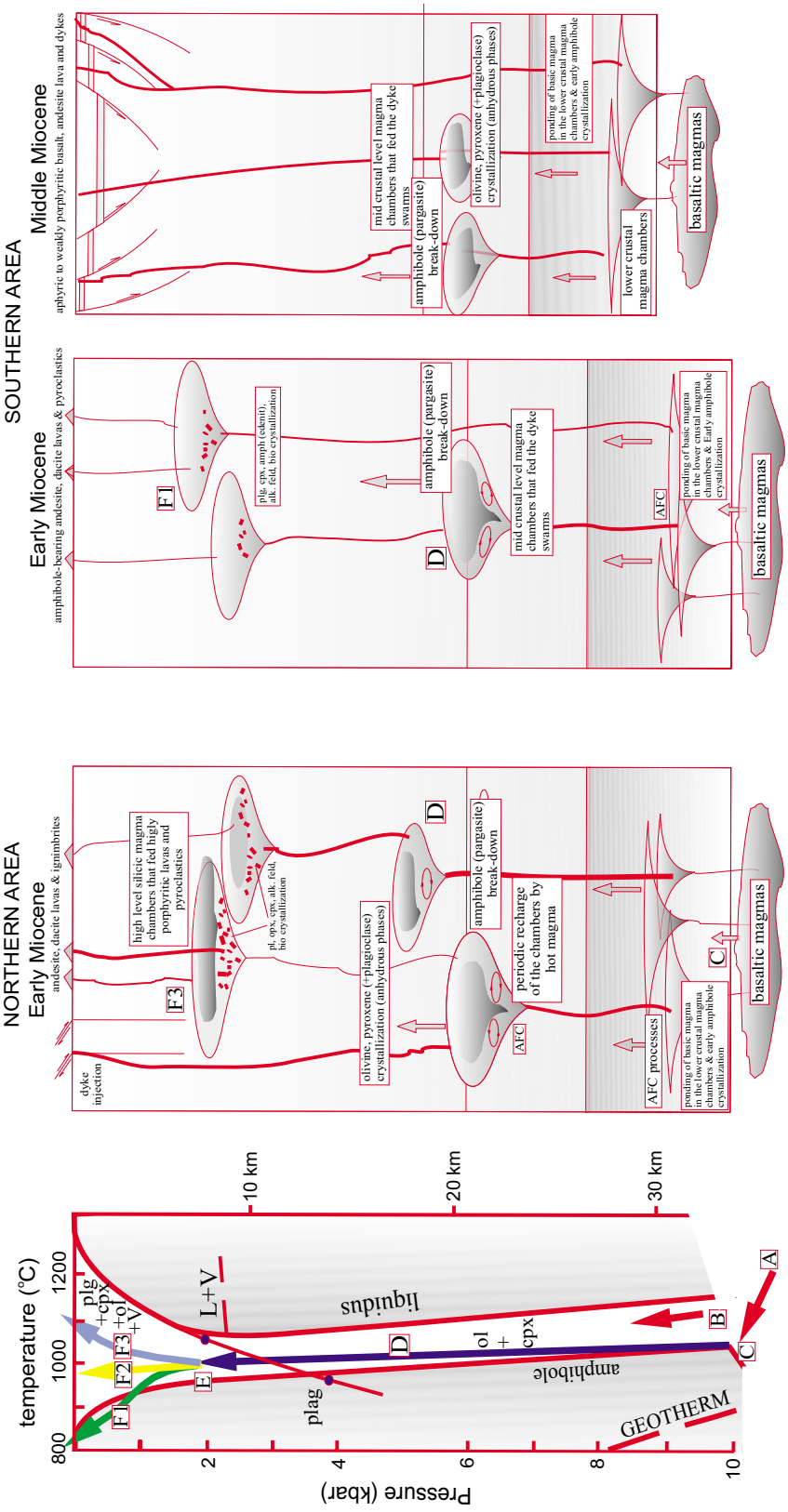

Figure 10. Schematic illustration of inferred mechanism for the evolution of magma batches within the crustal magma chambers of western Anatolia. The phase diagram is taken from Foden & Green (1992).

gradient of the magma becomes significantly less than the gradient of the amphibole-out reaction (point D in Figure 10). As a consequence, the early-formed pargasitic amphiboles break down as a result of decompressive, incongruent melting, eventually forming corona-textured xenoliths or being completely resorbed. The resultant crystalline assemblages are either pyroxene- or olivine-dominated (with plagioclase). The estimated pressures for the rocks of the dyke swarms range from 4.8 to 5.2 kbar at crystallization temperatures of 914–1086 °C. This suggests that the pyroxenes (with plagioclase and minor olivine) crystallized in mid-crustal magma chambers at a depth of about 16–20 km, corresponding to point D in Figure 10. Petrographic observations indicate that magmas in these magma chambers crystallized anhydrous phases such as plagioclase and pyroxene with minor olivine because amphibole was not an equilibrium phase at these *P-T* conditions.

The cooling paths that produce amphibole-free crystallization assemblages would be either F2 or F3 (Figure 10). The former suggests continuous adiabatic decompression and cooling, and ascending magma in equilibrium with amphibole at depth, and may simply erupt with an anhydrous pyroxene-feldspar assemblage insofar as the ascending path will not cross the amphibole-out curve; the later indicates possible late-stage heating. Resorption of plagioclase phenocrysts further indicates late-stage heating, which may be a result of either an entrainment of hotter mafic magmas by cooler felsic magmas during eruption of layered magma chambers, or release of latent heat of crystallization during enforced decompressive precipitation of plagioclase. In either case, the late-stage heating would cause amphibole instability (or partial resorption) and the crystallizing phases would be represented by plagioclase- and pyroxene-dominated and amphibole-free assemblages (similar to those observed in many of the lavas and dykes from the northern area).

Crystallization pressure estimates, constrained by the presence of biotite, indicate that the majority of the porphyritic lavas of the northern area were derived from magma chambers located at 10–14 km depths. These magma chambers are shown as high-level silicic magma chambers in Figure 10, because their products are dominantly acidic-intermediate rocks. The crystallizing assemblages in these magma chambers are generally plagioclase-dominated with two pyroxenes, K-feldspar and biotite. Foden & Green (1992) argued that magmas become plagioclase normative after fractionation of clinopyroxene and olivine at point D (Figure 10). Thus, the magma chambers near point D probably fed the high-level magma chambers as the magmas ascending to high-level silicic chambers should already have crystallized clinopyroxene and olivine in the mid-crustal chambers. In the high-level chambers, further assimilation of crustal material became quite limited, probably due to the fact that the magmas do not have enough energy to assimilate the crust significantly (Aldanmaz *et al.* 2000). As a result, the most important evolutionary process becomes fractional crystallization, which produces large volumes of acidic magmas with source geochemical signatures similar to those of the mafic-intermediate rocks of the dyke swarms (Aldanmaz *et al.* 2000).

In the southern area, the effects of amphibole fractionation become apparent via petrographic observations. The pressure estimates obtained from the Al-in hornblende geobarometer yield two different ranges of crystallization pressures for the acidic-intermediate Early Miocene rocks of the southern area. These are: (1) pressures of 7.1–8.6 kbar, which correspond to crystallization depths of 23–30 km; and (2) pressures of 2.1–4.2 kbar, which indicate crystallization depths of about 10–15 km. The early-formed amphiboles (mostly pargasitic) found in the porphyritic andesites and dacites in this area are compositionally identical to those found in the rocks of the northern area. This indicates that the early crystallization histories of the magmas of the two areas are similar. However, the existence of edenitic hornblende (the products of the shallow-level magma chambers) in the rocks of the southern area suggests a later crystallization which is different from the crystallization history of the rocks of the northern area. The results of experiments by Foden & Green (1992) suggest that the cooling paths of ascending magmas shallower than point E may change to produce smaller P/T slopes than those of the amphibole-out curve which they eventually re-cross (path F1 in Figure 10). In this case, hydrous evolved melts may re-cross the amphibole-out curve in shallow magma chambers and begin to fractionate amphibole to form the widely observed hornblende of the siliceous andesite and dacite. Elongate, quench-textured amphibole with lack of opacite resorption rims in the porphyritic lavas of the southern area are textural evidence, and the presence of green,

low-Al, high-Ti amphibole provides chemical evidence for this late-stage crystallization. Fractionation of amphibole and biotite in the more-evolved melt would derive fractionation from basaltic andesite through andesite to dacite. The presence of biotite suggests crystallization at relatively shallower depths, so this could possibly situate shallow magma chambers within the upper crustal levels. The temperature estimates, which fall in a range of 750–900 °C, also indicate low-temperature crystallization for the acidic-intermediate rocks of the southern area, consistent with the experimental results shown in Figure 10.

Amphibole xenocrysts with pargasitic composition are also observed in some of the Middle Miocene intermediate lavas and dykes of the southern area, indicating a similarly early fractionation history in the deep-level magma chambers (as in the Early Miocene rocks). The pressure estimates, however, suggest that the magmas that produced the Middle Miocene basic-intermediate rocks have not experienced fractionation in shallow-level magma chambers insofar as the crystallization pressures for these rocks are largely >6.5 kbar (Table 8). This interpretation is also consistent with the modelling of Aldanmaz *et al.* (2000) who used trace-element and isotopic characteristics of the rocks to demonstrate less contamination by crustal material and less fractionation of the Middle Miocene rocks relative to those of Early Miocene age. This can be attributed to regional extensional tectonics and progressive crustal thinning which led to the rapid movement of the magmas through the thinned and fractured crust. Rapid ascent of the magmas during the Middle Miocene period is also evident from the aphyric or weakly porphyritic nature of the Middle Miocene rocks.

Conclusions

The Early to Middle Miocene magmatic activity across western Anatolia produced a series of calc-alkaline and shoshonitic volcanic rocks that originated from a number of eruptive episodes. The rocks show a broad range of compositions, from basaltic to rhyolitic, and are composed of variable phenocryst assemblages. Application of mineral thermometry to the western Anatolian volcanic suites yielded pre-eruptive temperature estimates in the range of 585–1086 °C for the Early Miocene and 768–1095 °C for the Middle Miocene rocks. Pressures based on mineral barometry (clinopyroxene and Al-in-hornblende geobarometers) are in the range of 2.1–8.6 kbar for the Early Miocene and 6.5–9.1 kbar for the Middle Miocene rocks.

The presence of amphibole with clear signs of disequilibrium and plagioclase as inclusions in other phenocryst cores suggests that magma mixing played a significant role during the storage and ascent of magmas within crustal conduit systems. Strong compositional variations and reverse-zoning patterns within single phenocrysts, as well as considerably variable pressures of crystallization, further indicate that the magmas which produced the volcanic suite have polybaric origins and are the composite products of more than one petrogenetic stage. The observed range of phenocryst assemblages and the different compositional trends likely originated from fractionation of magmas under conditions of variable crystallization pressures.

Crystallization of amphibole – by reaction between hydrous melt and fractionated (e.g., cumulate) or wall-rock olivine and clinopyroxene – buffered melt compositions to basaltic andesite which fractionated hydrous mineral assemblages in deep crustal magma chambers near the crust-mantle transition. The primary magmas initially ponded in deep crustal reservoirs where they underwent combined fractional crystallization and crustal assimilation, or mixed with crustal melts. The early fractionation in deep magma chambers is likely to have performed the function of re-establishing the buoyant ascent of magma to form higher-level magma chambers with variable depths, sizes and fractionation assemblages.

Melt segregation occurred in high-level magmas chambers, and the more hydrous melts reached the amphibole stability field (for the case of the southern area), fractionating amphibole (and biotite) which drove the melt composition from basaltic andesite to dacite. These magmas erupted as andesitic to dacitic lava flows and domes with a crystallization assemblage having plagioclase + edenitic amphibole + pyroxene as major phases. Melts which did not fractionate amphibole (as in the case of the northern area) continued to fractionate plagioclase and evolved from basaltic andesite to andesite with some iron enrichment, evident from the widespread crystallization of orthopyroxene. These magmas predominantly form lava flows with the main fractionation phases of plagioclase + pyroxene(s). The

lack of amphibole fractionation in these magmas is interpreted to have resulted from possible late-stage heating. Resorption of plagioclase phenocrysts further suggests late-stage heating, which may have been a consequence of either an entrainment of hotter mafic magmas by cooler felsic magmas during eruption of a layered magma chamber, or of a release of latent heat of crystallization during enforced decompressive precipitation of phenocrysts.

Acknowledgements

The author would like to thank Julian Pearce for his comments, Pete Hill for providing access to the electron-microprobe facilities at the University of Edinburgh, and Stuart Kearns and Simon Burgess for their help during mineral analyses. A detailed review by Fatma Toksoy Köksal and editorial suggestions by Erdin Bozkurt helped to improve the clarity of the manuscript.

References

ALDANMAZ, E., PEARCE, J.A., THIRLWALL, M.F. & MITCHELL, J.G. 2000. Petrogenetic evolution of Late Cenozoic, post-collision volcanism in western Anatolia, Turkey. *Journal of Volcanology and Geothermal Research* **102**, 67–95.

ALDANMAZ, E. 2002. Mantle source characteristics of alkali basalts and basanites in an extensional intracontinental plate setting, western Anatolia, Turkey: implication for multi-stage melting. *International Geology Review* **44**, 440–457.

ALDANMAZ, E., GOURGAUD, A. & KAYMAKÇI, N. 2005. Constraints on the composition and thermal structure of the upper mantle beneath NW Turkey: evidence from mantle xenoliths and alkali primary melts. *Journal of Geodynamics* **39**, 277–316.

ALDANMAZ, E, KÖPRÜBAŞI, N., GÜRER, Ö.F., KAYMAKÇI, N. & GOURGAUD, A. 2006. Geochemical constraints on the Cenozoic, OIB-type alkaline volcanic rocks of NW Turkey: implications for mantle sources and melting processes. *Lithos* **86**, 50–76.

ALLEN, S.R. & CAS, R.A.F. 1998. Rhyolitic fallout and pyroclastic density current deposits from a phreatoplinian eruption in the eastern Aegean Sea. *Journal of Volcanology and Geothermal Research* **86**, 219–251.

ANDERSEN, D.J. & LINDSLEY, D.H. 1988. Internally consistent solution models for Fe-Mg-Mn-Ti oxides: Fe-Ti oxides. *American Mineralogist* **73**, 714–726.

ANDERSEN, D.J., LINDSLEY, D.H. & DAVIDSON, P.M. 1993. QUILF: a Pascal program to assess equilibria among Fe-Mg-Mn-Ti oxides, pyroxenes, olivine and quartz. *Computers and Geosciences* **19**, 1333–1350.

BACON, C.R. & HIRSCHMANN, M.M. 1988. Mg/Mn partitioning as a test for equilibrium between coexisting Fe-Ti oxides. *American Mineralogist* **73**, 57–61.

BAKER, D.R. & EGGLER, D.H. 1987. Compositions of anhydrous and hydrous melts coexisting with plagioclase, augite, and olivine or low-Ca pyroxene from 1 atm to 8 kbar: application to the Aleutian volcanic center of Atka. *American Mineralogist* **72**, 12–28.

BARCLAY, J. & CARMICHAEL, I.S.E. 2004. A hornblende basalt from western Mexico: water-saturated phase relations constrain a pressure-temperature window of eruptibility. *Journal of Petrology* **45**, 485–506.

BERMAN, R.G. 1988. Internally-consistent themodynamic data for minerals in the system Na_2O-K_2O-CaO-MgO-FeO-Fe_2O_3-Al_2O_3-SiO_2-TiO_2-H_2O-CO_2. *Journal of Petrology* **29**, 445–522.

BORSI, S., FERRARA, G., INNOCENTI, F. & MAZUOLI, R. 1972. Geochronology and petrology of recent volcanics in the eastern Aegean Sea. *Bulletin Volcanologique* **36**, 473–96.

BOWER, S.M. & WOODS, A.W. 1997. Control of magma volatile content and chamber depth on the mass erupted during explosive volcanic eruptions. *Journal of Geophysical Research* **102**, 10273–10290.

BOZKURT, E. 2001. Neotectonics of Turkey – a synthesis. *Geodinamica Acta* **14**, 3–30.

BOZKURT, E. & MITTWEDE, S.K. 2005. Introduction: evolution of continental extensional tectonics of western Turkey. *Geodinamica Acta* **18**, 153–165.

COUCH, S., SPARKS, R.S.J. & CARROLL, M.R. 2001. Mineral disequilibrium in lavas explained by convective self-mixing in open magma chambers. *Nature* **411**, 1037–1039.

DAVIDSON, J.P., TEPLEY, F.J. & KNESEL, K.M. 1998. Crystal isotope stratigraphy: a method for constraining magma differentiation pathways. *EOS* **79**, 185–189.

DEWEY, J.F., HEMPTON, M.R., KIDD, W.S.F., ŞAROĞLU, F. & ŞENGÖR, A.M.C. 1986. Shortening of continental lithosphere: the neo-tectonics of eastern Anatolia – a young collision zone. *In*: COWARD, M.P. & RIES, A.C. (eds), *Collision Tectonics*. Geological Society, London, Special Publications **19**, 3–36.

DUNGAN, M.A. & RHODES, J.M. 1978. Residual glasses and melt inclusions in basalts from DSDP Legs 45 and 46: evidence for magma mixing. *Contributions to Mineralogy and Petrology* **67**, 417–431.

ERCAN, T., SATIR, M., KREUZER, H., TÜRKECAN, A., GÜNAY, E., ÇEVİKBAŞ, A., ATEŞ, M. & CAN, B. 1984. Batı Anadolu Senozoyik volkanitlerine ait yeni kimyasal, izotopik ve radyometrik verilerin yorumu [Interpretation of new chemical, isotopic and radiometric data on Cenozoic volcanics of western Anatolia]. *Geological Society of Turkey Bulletin* **28**, 121–136 [in Turkish, with English abstract].

ERCAN, T., SATIR, M., STEINITZ, G., DORA, A., SARIFAKIOĞLU, E., ADIS, C., WALTER, H.J. & YILDIRIM, T. 1995. Biga Yarımadası ile Gökçeada, Bozcaada ve Tavşan adalarındaki (KB Anadolu) Tersiyer volkanizmasının özellikleri [Characteristics of the Tertiary volcanism of the Biga Peninsula, Gökçeada, Bozcaada and Tavşanadası, western Anatolia]. *Mineral Research and Exploration Institute of Turkey (MTA) Bulletin* **117**, 55–86 [in Turkish, with English abstract].

ERKÜL, F., HELVACI, C. & SÖZBİLİR, H. 2005. Stratigraphy and geochronology of the Early Miocene volcanic units in the Bigadiç borate basin, western Turkey. *Turkish Journal of Earth Sciences* **14**, 227–253.

FODEN, J.D. & GREEN, D.H. 1992. Possible role of amphibole in the origin of andesite: some experimental and natural evidence. *Contributions to Mineralogy and Petrology* **109**, 479–493.

GAMBLE, R.P. & TAYLOR, L.A. 1980. Crystal/liquid partitioning augite: effects of cooling rate. *Earth and Planetary Science Letters* **47**, 21–33.

GAETANI, G.A., GROVE, T.L. & BRYAN, W.B. 1993. The influence of water on the petrogenesis of subduction-related igneous rocks. *Nature* **365**, 332–334.

GILL, J.B. 1981. *Orogenic Andesites and Plate Tectonics.* Springer, Berlin.

GINIBRE, C., WORNER, G. & KRONZ, A. 2002. Minor- and trace-element zoning in plagioclase: implications for magma chamber processes at Parinacota volcano, northern Chile. *Contributions to Mineralogy and Petrology* **143**, 300–315.

GREEN, T.H. 1982. Anatexis of mafic crust and high pressure crystallisation of andesite. *In*: THORPE, R.S. (ed), *Orogenic Andesites*. Wiley, Chichester, U.K., 465–487.

GRUNDER, A.L. & MAHOOD, G.A. 1988. Physical and chemical models of zoned silicic magmas: the Loma Seca Tuff and Calabozos Caldera, South Andes. *Journal of Petrology* **29**, 831–867.

GÜLEÇ, N. 1991. Crust–mantle interaction in western Turkey: implications from Sr and Nd isotope geochemistry of Tertiary and Quaternary volcanics. *Geological Magazine* **128**, 417–435.

HAWTHORNE, F.C. 1981. Crystal chemistry of amphiboles, *In*: VEBLEN, D.R. (ed), *Amphiboles and Other Hydrous Pyroboles-Mineralogy*. Chelsea, Michigan, USA, 1–95.

HELZ, R.T. 1973. Phase relations of basalts in their melting ranges at pH_2O = 5 kb as a function of oxygen fugacity, Part I. Mafic phases. *Journal of Petrology* **14**, 249–302.

HEUBNER, J.S. & SATO, M. 1970. The oxygen fugacity-temperature relationships of manganese oxides and nickel oxide buffers. *American Mineralogist* **55**, 934–952.

HIBBARD, M.J. 1981. The magma mixing origin of mantled feldspars. *Contributions to Mineralogy and Petrology* **76**, 158–170.

HILDRETH, W. & MOORBART, S. 1988. Crustal contributions to arc magmatism in the Andes of southern Chile. *Contributions to Mineralogy and Petrology* **98**, 455–489.

HOLLAND, T.J.B. & BLUNDY, J. 1994. Non-ideal interactions in calcic amphiboles and their bearing on amphibole-plagioclase thermometry. *Contributions to Mineralogy and Petrology* **116**, 433–447.

HORT, M. 1998. Abrupt change in magma liquidus temperature because of volatile loss or magma mixing; effects on nucleation, crystal growth and thermal history of the magma. *Journal of Petrology* **39**, 1063–1076.

HOUSH, T.B. & LUHR, J.F. 1991. Plagioclase-melt equilibria in hydrous systems. *American Mineralogist* **76**, 477–492.

IRVINE, T.N. & BARAGAR, W.R.A. 1971. A guide to the chemical classification of the common volcanic rocks. *Canadian Journal of Earth Sciences* **8**, 523–448.

KELLER, J. 1983. Potassic volcanism in the Mediterranean area. *Journal of Volcanology and Geothermal Research* **18**, 321–325.

KONTAK, D.J., CLARK, A.H. & PEARCE, T.H. 1984. Recognition of simple and complex zoning in olivine and orthopyroxene phenocrysts using laser interference microscopy. *Mineralogical Magazine* **48**, 547–550.

KÖPRÜBAŞI, N. & ALDANMAZ, E. 2004. Geochemical constraints on the petrogenesis of Cenozoic I-type granitoids in Northwest Anatolia, Turkey: evidence for magma generation by lithospheric delamination in a post-collisional setting. *International Geology Review* **46**, 705–729.

LEAKE, B.E., WOOLLEY, A.R., ARPS, C.E.S., BIRCH, W.D., GILBERT, M.C., GRICE, J.D., HAWTHORNE, F.C., KATO, A., KISCH, H.J., KRIVOVICHEV, V.G., LINTHOUT, K., LAIRD, J., MANDARINO, J.A., MARESCH, W.V., NICKEL, E.H., ROCK, N.M.S., SCHUMACHER, J.C., SMITH, D.C., STEPHENSON, N.C.N., UNGARETTI, L., WHITTAKER, E.J.W. & GUO, Y.Z. 1997. Nomenclature of amphiboles: report of the subcommittee on amphiboles of the International Mineralogical Association, commission on new minerals and mineral names. *American Mineralogist* **82**, 1019–1037.

LEBAS, M.J., LE MAITRE, R.W., STRECKEISEN, A. & ZANETTIN, B. 1986. A chemical classification of volcanic rocks based on the total alkali-silica diagram. *Journal of Petrology* **27**, 445–450.

LEPAGE, L.D. 2003. ILMAT: an Excel worksheet for ilmenite-magnetite geothermometry and geobarometry. *Computers and Geosciences* **29**, 673–678.

LINDSLEY, D.H. 1983. Pyroxene thermometry. *American Mineralogist* **68**, 477–493.

LINDSLEY, D.H. & ANDERSEN, D.J. 1983. A two pyroxene thermometer: Proceedings of the Thirteenth Lunar and Planetary Science Conference, Part 2. *Journal of Geophysical Research* **88**, Supplement, A887–906.

LUHR, J.F. & CARMICHAEL, I.S.E. 1980. The colima volcanic complex, Mexico. I. Post-caldera andesites from Volcan Colima. *Contributions to Mineralogy Petrology* **71**, 343–372.

MORIMOTO, N. 1989. Nomenclature of pyroxenes. *Canadian Mineralogist* **27**, 143–156.

MORRICE, M.G. & GILL, J.B. 1986. Spatial patterns in the mineralogy of island arc magma series: Sangihe Arc. Indonesia. *Journal of Volcanology and Geothermal Research* **29**, 311–353.

MYERS, J. & EUGSTER, H.P. 1983. The system Fe-Si-O: oxygen buffer calibrations to 1,500K. *Contributions to Mineralogy and Petrology* **82**, 75–90.

NANEY, M.T. 1983. Phase equilibria of rock-forming ferromagnesian silicates in granitic systems. *American Journal of Science* **283**, 993–1033.

NELSON, S.T. & MONTANA, A. 1992. Sieve-textured plagioclase in volcanic rocks produced by rapid decompression. *American Mineralogist* **77**, 1242–1249.

NIXON, G.T. & PEARCE, T.H. 1987. Laser-interferometry of oscillatory zoning in plagioclase: the record of magma mixing and phenocryst recycling in calc-alkaline magma chambers, Iztaccihuat Volcano, Mexico. *American Mineralogist* **72**, 1144–1162.

PANJASAWATWONG, Y., DANYUSHEVSKY, L.V., CRAWFORD, A.J. & HARRIS, K.L. 1995. An experimental study of the effects of melt composition on plagioclase–melt equilibria at 5 and 10 kbar: implications for the origin of magmatic high-An plagioclase. *Contributions to Mineralogy and Petrology* **118**, 420–432.

PUTIRKA, K.D., MIKAELIAN, H., RYERSON, F. & SHAW, H. 2003. New clinopyroxene-liquid thermobarometers for mafic, evolved, and volatile-bearing lava compositions, with applications to lavas from Tibet and the Snake River Plain, Idaho. *American Mineralogist* **88**, 1542–1554.

ROBERT, U., FODEN, J. & VARNE, R. 1992. The Dodecanese Province, SE Aegean: a model for tectonic control on potassic magmatism. *Lithos* **28**, 241–260.

ROEDER, P.L. & EMSLIE, R.F. 1970. Olivine-liquid equilibrium. *Contributions to Mineralogy and Petrology* **29**, 275–289.

RUTHERFORD, M.J., DEVINE, J.D. & BARCLAY, J. 1998. Changing magma conditions and ascent rates during the Soufriere. Hills eruption on Montserrat. *GSA Today* **8**, 1–7.

SCHMIDT, W.S. 1992. Amphibole composition in tonalite as a function of pressure: an experimental calibration of the Al-in hornblende barometer. *Contributions to Mineralogy and Petrology* **110**, 304–310.

ŞENGÖR, A.M.C. & YILMAZ, Y. 1981. Tethyan evolution of Turkey: a plate tectonic approach. *Tectonophysics* **75**, 181–241.

SEYİTOĞLU, G., ANDERSON, D., NOWELL, G. & SCOTT, B. 1997. The evolution from Miocene potassic to Quaternary sodic magmatism in western Turkey: implications for enrichment processes in the lithospheric mantle. *Journal of Volcanology and Geothermal Research* **76**, 127–147.

SISSON, T.W. & GROVE, T.L. 1993. Experimental investigations of the role of H_2O in calc-alkaline differentiation and subduction zone magmatism. *Contributions to Mineralogy and Petrology* **113**, 143–166.

SPARKS, R.S.J., BARCLAY, J., JAUPART, C., MADER, H.M. & PHILLIPS, J.C. 1994. Physical aspects of magmatic degassing I. Experimental and theoretical constraints on vesiculation. *In*: CARROLL, M.R. & HOLLOWAY, J.R. (eds), *Volatiles in Magmas.* Mineralogical Society of America, Reviews in Mineralogy **30**, 413–443.

TEPLEY, F.J., DAVIDSON, J.P., TILLING, R.I. & Arth, J.G. 2000. Magma mixing, recharge and eruption histories recorded in plagioclase phenocrysts from El Chichón Volcano, Mexico. *Contributions to Mineralogy and Petrology* **41**, 1397–1411.

TOKÇAER, M., AGOSTINI, S. & SAVAŞÇIN, M.Y. 2005. Geotectonic setting and origin of the youngest Kula volcanics (western Anatolia), with a new emplacement model. *Turkish Journal of Earth Sciences* **14**, 143–166.

TROLL, V.R. & SCHMINCKE, H.U. 2002. Magma mixing and crustal recycling recorded in ternary feldspar from compositionally zoned peralkaline ignimbrite 'A', Gran Canaria, Canary Islands. *Journal of Petrology* **43**, 243–270.

TSUCHIYAMA, A. 1985. Dissolution kinetics of plagioclase in the melt system diopside-albite-anorthite, and origin of dusty plagioclase in andesites. *Contributions to Mineralogy and Petrology* **89**, 1–16.

WYERS, G.P. & BARTON, M. 1987. Geochemistry of a transitional ne-trachybasalt – Q-trachyte lava series from Patmos (Dodecanese), Greece; further evidence for fractionation, mixing and assimilation. *Contributions to Mineralogy and Petrology* **97**, 279–291.

YILMAZ, Y., GENÇ, Ş.C., KARACIK, Z. & ALTUNKAYNAK, Ş. 2001. Two contrasting magmatic associations of NW Anatolia and their tectonic significance. *Journal of Geodynamics* **31**, 243–271.

YÜCEL-ÖZTÜRK, Y., HELVACI, C. & SATIR, M. 2005. Genetic relations between skarn mineralization and petrogenesis of the Evciler Granitoid, Kazdağ, Çanakkale, Turkey and comparison with world skarn granitoids. *Turkish Journal of Earth Sciences* **14**, 225–280.

Received 26 September 2005; revised typescript accepted 17 January 2006